

4

5

6

1

2

A Numerical Study on the Influences of Sumatra Topography and Synoptic Features on Tropical Cyclone Formation over the Indian Ocean

7

8

9

Chung-Chieh Wang¹, Shin-Kai Ma¹, and Richard H. Johnson²

1011

12 I Department of Earth Sciences, National Taiwan Normal University, Taipei, Taiwan
 13 2 Department of Atmospheric Sciences, Colorado State University, Fort Collins, CO, USA

1415

- Third revision for
- 17 Monthly Weather Review

18

19

20 April 2020

2122

- * Corresponding Author address: Prof. Chung-Chieh Wang, Department of Earth Sciences,
- National Taiwan Normal University. No. 88, Sec. 4, Ting-Chou Rd., Taipei, 11677 Taiwan. E-
- 25 mail: cwang@ntnu.edu.tw

Early Online Release: This preliminary version has been accepted for publication in *Monthly Weather Review*, may be fully cited, and has been assigned DOI 10.1175/MWR-D-19-0259.1. The final typeset copyedited article will replace the EOR at the above DOI when it is published.

Abstract

Spanning across the Equator with a northwest-southeast orientation, the island of
Sumatra can exert significant influences on low-level flow. Under northeasterly flow, in
particular, lee vortices can form and some of them may subsequently develop into tropical
cyclones (TCs) in the Indian Ocean (IO). Building upon the recent work of Fine et al. (2016),
this study investigates the roles of the Sumatra topography and other common features on the
formation of selected cases for analysis and numerical experiments.
Four cases in northern IO were selected for analysis and two of them [Nisha (2008) and
Ward 2009)] for simulation at a grid size of 4 km. Sensitivity tests without the Sumatra
topography were also performed. Our results indicate that during the lee stage, most pre-TC
vortices tend to be stronger with a clearer circulation when the topography is present.
However, the island's terrain is a helpful but not a deciding factor in TC formation.
Specifically, the vortices in the no-terrain tests also reach TC status, but just at a later time.
Some common ingredients contributing to a favorable environment for TC genesis are
identified. They include northeasterly winds near northern Sumatra, westerly wind bursts
along the equator, and migratory disturbances (TC remnants or Borneo vortices) to provide
additional vorticity/moisture from the South China Sea. These factors also appear in most of
the 22 vortices in northern IO during October-December in 2008 and 2009. For the sole case
(Cleo) examined in southern IO, the deflection of equatorial westerlies into northwesterlies by
Sumatra (on the windward side) is also helpful to TC formation

1. Introduction

The formation of a tropical cyclone (TC) is regarded as a complex process that involves
continuous and nonlinear interaction among mechanisms across a wide range of scales, rather
than controlled by a single mechanism. Since Ooyama (1982), tropical cyclogenesis is
considered the transition from the probabilistic to deterministic stage in the lifecycle of a TC.
In the probabilistic stage with weak relative vorticity ζ (and absolute vorticity η), tropical
cloud clusters typically have large Rossby radius of deformation (λ_R) and low heating
efficiency from latent heat release, and most of them have short lifespans and do not intensify
into TCs.
Past studies have established the synoptic conditions conducive to TC formation (e.g.,
Gray 1968): deep ocean mixing layer with sea-surface temperature (SST) at least 26.5°C,
unstable atmospheric environment, high moisture content in low and middle levels, weak
vertical wind shear, a latitude outside 5° (nonzero Coriolis force), and high low-level vorticity.
However, even when all the above conditions are met in the probabilistic stage, it only means
a higher likelihood for TC genesis. The cloud cluster (and initial vortex) still needs external
forcing mechanism(s) to increase its vorticity, reduce the λ_R , and subsequently raise the
heating efficiency of latent heat released in cumulus convection. Only after that, the
disturbance can survive the probabilistic stage and enter the deterministic stage with positive
feedback in development through the mechanisms of angular momentum conservation and
Conditional Instability of the Second Kind (CISK; Charney and Eliassen 1964) or Wind-
Induced Surface Heat Exchange (WISHE; Emanuel 1986; Rotunno and Emanuel 1987).
For individual disturbances, some external forcing mechanism, or mechanisms, is an
essential element for TC formation, besides favorable environmental conditions. In the
western North Pacific (WNP), for example, Ritchie and Holland (1999) identified five large-
scale circulation features or processes that can force or are linked to TC formation: monsoon

shear lines, monsoon gyres, easterly waves, monsoon confluence regions, and Rossby energy
dispersion. The observational study of Lee (1986) also points out the importance of low-level
momentum forcing in TC-genesis cases in the WNP. Such momentum forcing over a large
area may come from cross-equatorial flow, trade wind surges, or bursts of the Indian
monsoon. Through inward transfer of eddy vorticity flux, the forcing can increase the low-
level ζ of the TC vortex without a strengthening in its transverse circulation, and act to help
the TC to enter the deterministic stage (Lee 1986).
Mid-latitude cold-air outbreaks in the opposing hemisphere are usually the source of the
cross-equatorial flow (Love 1985a,b), while those in the same hemisphere can initiate trade
wind surges. In northern Indian Ocean (NIO) where TCs occur more often during pre-
monsoon and post-monsoon seasons (e.g., Subbaramayya and Rao 1984; Kikuchi and Wang
2010), similar low-level momentum forcings from wind bursts also often promote TC
formation there (Lee et al. 1989). In these situations, initially asymmetric shearing vorticity
gradually turns into symmetric curvature vorticity as the vortex strengthens. In addition, when
a TC forms and intensifies in the IO, its outer circulation can enhance the shearing vorticity in
the other hemisphere and this process may lead to TC formation there, resulting in a TC pair
across the equator (Lee et al. 1989).
The cold surge helps TC formation not only in WNP and NIO, but also in the South
China Sea (SCS; Chang et al. 2004; Lin and Lee 2011). In the winter, when the northeasterly
wind surge reaches the SCS, it may provide positive vorticity and lead to the formation of the
Borneo vortex (BV). Some semi-stationary and others westward-moving, these BVs may
continue to develop and eventually become a TC if the environment is favorable (Lin and Lee
2011). One such example is Typhoon Vamei (2001) that formed near Singapore very close to
the equator (Chang et al. 2003). Through composite analysis, Takahashi et al. (2011) also
found that regions of positive vorticity often exist in the SCS and NIO due to strong

northeasterly flow during the winter months (October-March), thus contributing to TC formation in these ocean basins.

97

98

99

100

101

102

103

104

105

106

107

108

109

110

111

112

113

114

115

116

117

118

119

120

121

In addition to the large-scale momentum forcing mentioned above, certain topographic features in the tropics, when encountered by airflow, can act to produce localized vorticity, and therefore play a role in TC formation. One such feature is Central America (the Sierra Madre range in particular), which is argued to affect the formation of hurricanes downstream from the topography in eastern North Pacific (Mozer and Zehnder 1996; Farfán and Zehnder 1997; Zehnder et al. 1999). Results from numerical experiments indicate that lee vortices (Smolarkiewicz and Rotunno 1989; Rotunno and Smolarkiewicz 1991; Epifanio 2003), with a depth of about 3 km, often form downstream of Central America in a low-Froude number (Fr) regime under easterly prevailing wind. The definition of Fr, which gives the overall response of the flow when encountering an obstacle, is Fr = U/Nh, where U is the wind speed perpendicular to the topography, N is buoyancy oscillation frequency, and h is the terrain height. For Central America, both a strong jet through the Tehuantepec gap and flow around topography can produce vorticity to form lee vortices under such conditions. With moisture advection from the Intertropical Convergence Zone (ITCZ), the environment downstream from Central America may become even more favorable to TC development (Zehnder et al. 1999). The above case studies indicate the topography can produce the initial vortex, which can develop into a TC given a suitable environment.

Compared to Central America, the topography of Sumatra at the western end of maritime continent is much less studied. Kuettner (1967, 1989) suggests that the unique configuration of Sumatra, which straddles the equator in a way that is found nowhere else in the world, may be an important source for TC pairs in the IO. With a northwest-southeast orientation, the topography of Sumatra extends more than 1600 km (from about 6°N to 6°S) and peaks at about 3.8 km (cf. Fig. 1a). When the winter northeasterly flow reaches Sumatra, lee vortices

may form at both ends. While counter-rotating, both are cyclonic and may serve as initial
vortices and, after shedding, intensify into TCs under a favorable environment (Fig. 1a).
Recently, Fine et al. (2016) examined TCs in the IO using datasets from European Center

for Medium-Range Weather Forecasts (ECMWF) Year of Tropical Convection (YOTC, 2008-2010; Waliser et al. 2012) and Dynamics of the Madden-Julian Oscillation (DYNAMO, 2011-2012; Johnson and Ciesielski 2013). They found that 31.3% of all TCs in the 2.5-yr study period in NIO can be traced back to the Sumatra area, while the corresponding number for the southern IO (SIO) is 22.9%. These high percentages imply that the topography of Sumatra could play a significant role in providing initial vortices of TCs in IO. For northern (southern) Sumatra, the terrain-induced cyclonic vortices are more common during boreal winter (summer) with low-level easterly flow, while TC genesis from them in NIO appear to occur in October-December (Fine et al. 2016), presumably linked to other environmental factors.

Following Fine et al. (2016), which is a preliminary observational and climatological study without an examination on the TC genesis of individual cases, a numerical study seems logical. Therefore, the present study selects a few lee vortex cases during the YOTC period for analysis and numerical simulation. Sensitivity experiments in which the Sumatra topography is removed are also performed, with a goal of clarifying the importance of the topography relative to other potentially helpful factors for TC formation in these cases. These other factors include synoptic ingredients surrounding the lee area as well as vorticity and moisture advection associated with incipient disturbances, such as a BV, from the SCS upstream. This study represents the first numerical investigation of the processes involved in TC formation associated with Sumatra wake vortices as well as the relative importance of other synoptic features in the environment.

2. Data and design of numerical experiments

a. Data and analysis methods

147

148

149

150

151

152

153

154

155

156

157

158

159

160

161

162

163

164

165

166

167

168

169

170

171

In this study, all the TCs in the NIO during October-December within the YOTC period (May 2008-April 2010, Waliser et al. 2012; Moncrieff et al. 2012) are briefly analyzed (sections 3 and 6), and their basic track and intensity information was taken from the Joint Typhoon Warning Center (JTWC) best-track data. The gridded ECMWF-YOTC global analyses (e.g., Moncrieff et al. 2012), available on a $0.25^{\circ} \times 0.25^{\circ}$ (latitude-longitude) grid at 20 levels (1000 to 10 hPa) every 6 h, are used for the examination of the synoptic environment and evolution of these storms. From the 13 cases included in Fine et al. (2016), five TCs that could be linked to Sumatra (during October-December) were selected for a more detailed analysis of the processes of lee vortex formation and the subsequent TC genesis using the ECMWF-YOTC data in section 3. The three stronger TCs, including Nisha (2008) and Ward (2009) in the NIO and Cleo (2009) in the SIO, that became named storms are further chosen for numerical simulation and sensitivity tests. The ECMWF-YOTC data serve as initial and boundary conditions (IC/BCs) for these experiments. Satellite brightness temperature (T_B) imageries provided by the Naval Research Laboratory (NRL) and microwave products from the Space Science and Engineering Center (SSEC, at University of Wisconsin) are also used to help verify model simulations. In this study, the intensity of tropical storm (TS) of 34 kts is adopted to identify TC formation in both the observation and model in a consistent way, as the storms are given a name and typically enter the deterministic stage near this time (Ooyama 1982). To analyze their vertical structure and evolution, the centers of the vortices at (or near) 850 hPa are identified and used to compute the mean relative vorticity within 550 km, a radius determined after extensive testing, including the earlier, lee stage of the vortices. To further diagnose the

differences between the control experiment and sensitivity test (without the Sumatra terrain)

of each TC case, the vorticity equation was employed, and a lag correlation analysis between the vorticity of the lee vortex and the upstream Fr was also carried out to elucidate the topographic effects of the Sumatra Island. Further details of these analyses will be described in sections 4 and 5.

b. Numerical model and experiments

172

173

174

175

176

177

178

179

180

181

182

183

184

185

186

187

188

189

190

191

192

193

194

195

196

The Cloud-Resolving Storm Simulator (CReSS) version 3.4.2 (Tsuboki and Sakakibara 2002, 2007) is used in this study for all experiments. It is a single-domain, non-hydrostatic and compressible cloud-resolving model with a terrain-following vertical coordinate. In CReSS, clouds are explicitly treated using a bulk cold-rain microphysics scheme with a total of six species (vapor, cloud water, cloud ice, rain, snow, and graupel) without the use of any cumulus parameterization, while subgrid-scale processes such as turbulent mixing in the boundary layer and surface radiation and momentum/energy fluxes are parameterized (Table 1). The CReSS model has been employed in many earlier studies on TCs (Wang 2015; Wang et al. 2012; 2013; 2015; 2016; Chen et al. 2017; Kuo et al. 2019), and the readers are referred to the references therein and Tsuboki and Sakakibara (2002, 2007) for further details. Two control (CTL) experiments were performed using a large domain of 5600 km × 4464 km (roughly 20°S-20°N, 70°-120°E, Fig. 1b) at a convective-permitting grid size of 4 km, one for Nisha (2008) and the other for Ward (2009) and Cleo (2009) together, since they were twin cyclones across the equator during the same period. Using the YOTC analyses as IC/BCs, these runs started from 6 h before the arrival of low-level northeasterly flow to Sumatra, at 1200 UTC 14 November 2008 for Nisha and 0000 UTC 29 November 2009 for Ward and Cleo, and lasted for 15 and 16 days, respectively (Table 1). For the no-terrain (NT) tests, all model setups and IC/BCs are identical to the CTL, except that the topography of Sumatra (and the small islands nearby) are removed (but the land mass remains, cf. Fig. 1a).

Here, it should be noted that the SIO case of Cleo was not a lee vortex, since the northeasterly

197 flow did not extend south of the equator. In fact, none of the SIO TCs examined by Fine et al.

(2016) developed from a lee vortex, but as the only SIO case, it is still worthwhile to include

199 Cleo in the present study.

198

- 200 c. Vorticity budget analysis for lee vortices
- Except for the methods mentioned above in section 2a, the vorticity budget analysis was
- also performed for the vortices during the lee stage in both CTL and NT experiments for each
- of the selected cases to further shed lights on their development. The vorticity (tendency)
- 204 equation in Cartesian and z coordinate can be written as

$$205 \qquad \frac{\partial \zeta}{\partial t} = -\vec{\mathbf{V}} \cdot \nabla \eta - w \frac{\partial \zeta}{\partial z} - \eta \left(\nabla \cdot \vec{\mathbf{V}} \right) + \left(\frac{\partial u}{\partial z} \frac{\partial w}{\partial y} - \frac{\partial v}{\partial z} \frac{\partial w}{\partial x} \right) + \frac{1}{\rho^2} \left(\frac{\partial \rho}{\partial x} \frac{\partial p}{\partial y} - \frac{\partial \rho}{\partial y} \frac{\partial p}{\partial x} \right) + \left(\frac{\partial F_y}{\partial x} - \frac{\partial F_x}{\partial y} \right) \tag{1}$$

- where the forcing terms on the RHS, following the order, are horizontal advection of $\eta = \zeta +$
- 207 f), vertical advection of ζ , convergence (or vertical stretching) effect, tilting effect, solenoidal
- effect, and the frictional effect that also accounts for the residual from computational errors.
- 209 Using Eq. (1), the model results of lee vortices in CTL and NT experiments are compared
- 210 (sections 4 and 5).

211

212

3. Case analysis

- The five TCs linked to Sumatra during the data period were selected for analysis in this
- section, and they are TC 03A (2008), TS Nisha (2008), TC 07B (2008), TS Ward (2009), and
- 215 TC Cleo (2009), respectively, in chronological order. The first four were in the NIO and
- developed into TCs from lee vortices of northern Sumatra, while Cleo was in the SIO and
- formed a TC pair with Ward as mentioned. The full tracks of these five cases, constructed
- using both YOTC analysis (vortex center at 850 hPa during pre-TS stage) and JTWC best-
- track data (TS and beyond), are shown in Fig. 1b.
- Following the methodology described in section 2a, time-height sections of mean

relative vorticity ζ inside a radius of 550 km for the four cases in NIO were constructed (Fig.
2). This allowed us to identify the level of maximum (areal-mean) ζ during the leeside stage
of the vortices, and these levels were used to show (in Fig. 3) the evolution in wind and
vorticity before, during, and after the formation of leeside vortex (t_0) , which is taken to be the
time when a closed circulation at 850 hPa formed in the ECMWF-YOTC analysis. During the
4-day period, easterly flow appeared near northern Sumatra and to its north in all four cases
and generally strengthened during the period (Fig. 3). At the same time, westerly winds
intensified at lower latitudes near the equator prior to t_0 , except for 03A in which westerlies
occurred shortly after t_0 (Fig. 3a). Appearing also in the composite fields of Fine et al. (2016,
their Figs. 2a and 6), these two branches of airflow provided cyclonic vorticity and a
background environment favorable for lee vortex formation and its subsequent development.
In addition to the opposing flow in the leeside region, clear incipient positive vorticity
also existed in Fig. 3 near 110°E at 0°-5°N in the SCS two days before lee vortex formation in
all three latter cases, while the one in 03A was weaker and less evident (Fig. 3a). Note that
03A is the only case among the four that did not reach TS status (cf. Fig. 2a). These vorticity
centers were either from the remnants of tropical systems or associated with a BV and moved
westward to reach the leeside of northern Sumatra at t_0 , when the lee vortex subsequently
formed. Afterward, the lee vortex in all four cases gradually shed and moved downstream,
away from Sumatra (Figs. 1a and 3). In longitude-time (Hovmöller) plots (Fig. 4), the
incipient disturbances can be identified to be from the remnants of TS Maysak for Nisha,
while there are possibly some linkages with the remnants of a tropical depression for 03A,
and a BV for both 07B and Ward, respectively. These precursor systems also carried a higher
moisture content (in total precipitable water) into the lee area or its vicinity (Fig. 4, right
column). For the latter two cases, the vorticity associated with the incipient BV was stronger
with a wider circulation (Figs. 3c,d) and maximized farther aloft near 500-600 hPa around t_0

(Figs. 2c,d). As the vortex moved downstream afterwards, it developed downward toward the surface and the low-level ζ strengthened (Fig. 2). Apparently, these migratory synoptic disturbances provided incipient vorticity and moisture and were also helpful to the development of lee vortex, and subsequently the TC at a later time (e.g., Gray 1968).

Figure 5 presents the 925-hPa flow fields and precipitable water amount in a larger domain at t_0 for the four NIO cases. Except for 03A, which had a weaker flow, strong northeasterly or northerly winds from cold air surges from mid-latitudes were present over much of the SCS and Malay Peninsula in the other three cases (Figs. 5b-d). The relatively dry cold air became easterly as it traveled south and reached the northern tip of Sumatra at this time. Meanwhile, along the equator, there existed a westerly wind burst (WWB) of 5-20 m s⁻¹ at low-levels in these three cases. Interestingly, a pair of synoptic-scale vortices were also present across the equator in the IO (red dashed circles in Fig. 5) in each case, and their circulations (with enhanced horizontal pressure gradients) possibly helped the equatorial westerlies to intensify, in a way previously pointed out by Lee et al. (1989).

In all four cases, low-level southeasterly flow prevailed over a vast area south and southwest of Sumatra (Fig. 5). Coupled with the westerly flow (or a weaker flow) along the equator, this provided cyclonic vorticity (in the Southern Hemisphere) for the region west of southern Sumatra, as shown in Figs. 5a,c,d (green dashed circles), also consistent with Lee et al. (1989) and Fine et al. (2016, their Fig. 7). The vortex west of southern Sumatra in Fig. 5d later developed into Cleo, which formed a vortex pair with Ward. As mentioned, the remnants of western Pacific tropical disturbances or BVs were associated with higher moisture content in the SCS (white dashed circles in Fig. 5) at this time (for Nisha, 07B, and Ward), and would soon move into the leeside of northern Sumatra.

Thus, some common precursor synoptic-scale features or ingredients can be identified from Figs. 3-5 for the four TC cases in NIO. They include low-level northeasterly wind surges

in the SCS, WWBs along the equator to the west of Sumatra, and an incipient disturbance that brought stronger relative vorticity and higher moisture content into the lee area through horizontal advection. Among these features, the equatorial westerly winds were most likely also enhanced by vortex pairs across the equator when they developed. Below, the two stronger cases that became named storms, i.e., TS Nisha (2008) and TC Ward (2009), are further selected for numerical simulation and an investigation to assess the relative importance of the topography of Sumatra, in particular to the subsequent TC formation. To achieve this goal, both CTL and NT experiments were performed for each case, and their results are compared in the following section.

4. Model results of Nisha and Ward in the northern Indian Ocean

a. Tropical Storm Nisha (2008)

For each case, the CTL experiment needs to be validated against the observations to ensure that the event is reproduced reasonably well. First, the modeled track and intensity for Nisha (2008) are shown in Fig. 6. Overall, the simulated track is fairly close to the track in the YOTC data, and the vortex first forms at the leeside of northern Sumatra and then moves westward and northwestward toward Sri Lanka and southern India, despite some discernible differences (Fig. 6a). In particular, the landfall points in Sri Lanka and southeastern India in CTL are quite close to the observation, an encouraging result for a model run 15 days in length. Similarly, reasonable results are obtained by the model for the intensity of Nisha (Fig. 6b). In CTL, the timing to reach TS intensity (34 kts) is only about 1.5 days earlier than the JTWC data, while the modeled peak intensity (54 kts) on 26 November is also very close to the best track (50 kts). A deficit of about 10 hPa in the TC's minimum mean sea-level pressure (MSLP) appears after Nisha reached TS status, when the JTWC best track suggested 985 hPa (Fig. 6c). Thus, the central MSLP in CTL is only about 5-10 hPa lower than the YOTC data,

but the peak wind speed is considerably stronger (by nearly 20 kts) and close to the JTWC data due to the high resolution of the model. At early stages before TS, the maximum wind speed in CTL is also consistently stronger than the YOTC. Overall, the simulation in track and intensity for Nisha is quite reasonable.

In Fig. 7, the model outputs of the column-maximum mixing ratio of precipitation (rain, snow, plus graupel) and low-level winds (at 1547 m) are compared to the SSMI brightness temperature for deep convection and rainband structure of TS Nisha and the YOTC winds at 850 hPa, at selected times of similar evolutionary stage. Even though the two quantities for convection are not identical, the figure provides verification that the model well-reproduced the storm structure of Nisha before and during its TS stage since 23 November. For example, the convection was quite loose and more scattered when the storm first approached Sri Lanka (Figs. 7a,e), became more organized but asymmetrical (more in the northern quadrants) on 24 November (Figs. 7b,f), then further tightened in cloud structure on the approach to southern India (Figs. c,d and g,h). Overall, the simulation agrees very well with the observation in cloud patterns and low-level circulation.

The time-height section (0-12.3 km) of ζ for the vortex in CTL, also averaged inside 550 km from the center, is presented in Fig. 8a and can be compared with Fig. 2b from the YOTC data for their general characteristics. Overall, the two plots are similar in both the magnitude and vertical structure of the areal-mean ζ , but some differences still exist. For example, the model vortex appears weaker than that in the ECMWF-YOTC analyses in the lower levels during its leeside stage, but not so when one compares peak wind speed or central MSLP (cf. Fig. 6). After the vortex starts to shed, the CTL result agrees closely with the ECMWF in areal-mean ζ (Figs. 2b and 8a), and Nisha in CTL reaches TS intensity at 0000 UTC 24 November, roughly 42 h before the time issued by JTWC (Fig. 6b) as mentioned.

When the terrain of Sumatra is removed in the NT experiment, the simulated track

remains close to that in CTL (Fig. 6a). At first glance, the time-height ζ inside 550 km for
Nisha in the two runs also appear similar, including the lee stage (Figs. 8a,b). Their
differences, many quite subtle, can be better depicted in Fig. 8c (CTL minus NT), where the
areal-mean ζ at low levels in CTL tends to be stronger than that in NT for much of the time
since 17 November, especially over 21-26 November as the vortex strengthens to reach the TS
status. In agreement with Fig. 8c, the near-surface flows (below 1 km) in CTL also produce a
stronger vorticity belt and a clearer vortex circulation center on 21 November (figure not
shown). This result is consistent with Epifanio and Durran (2001), who suggest that
topography can form corner flow and provide stronger shear vorticity to the downstream area.
With a weaker mean ζ , the maximum wind speed associated with Nisha in NT is weaker than
that in CTL over 21-27 November (Fig. 6b), often by 5-10 kts, and the storm reaches TS
intensity on 25 November, more than one day (27 h) later than in CTL. Even though the storm
in CTL is stronger through much of its lifespan (Figs. 6b,c), the one in NT also reaches TS
status when the topography of Sumatra is removed.
To gain insight into the development of the lee vortex in CTL and to contrast it with the
one in NT, a vorticity budget analysis (cf. section 2c) is performed on the vortex at a height of
1547 m (near 850 hPa), averaged also inside a radius of 550 km from the center, for its lee
stage as shown in Fig. 9. For the pre-Nisha lee vortex in CTL (1200 UTC 15 to 0000 UTC 18
November 2008, $t = 24-84$ h), it is seen that the mean ζ at 1547 m (dashed curve with dots)
generally increases with time during this 60-h period, roughly from 0.8 to $1.7 \times 10^{-5} \text{ s}^{-1}$ (Fig.
9a), mainly contributed by two terms: convergence/stretching (green) and vertical advection
(brown). The convergence effect is counteracted (out of phase) by horizontal advection (blue)
as the same low-level inflow also tends to bring in lower ζ values from larger radii, while the
vertical advection is largely cancelled by the tilting term (red) since the stronger upward
motion at the vortex center also tilts the vorticity vector from the vertical (rotation on xy-

plane) into horizontal direction (rotation on vertical plane). While all the above four terms
reach around $2 \times 10^{-9} \ s^{-2}$ in their peak magnitude, the friction/residual term is significantly
smaller and the solenoidal effect is negligible. As a result, the local tendency of ζ in Fig. 9a
(computed using time differentiation) is a relatively small net difference among the larger
RHS terms with opposite signs, but is mostly positive to cause the gradual increase in ζ .
During 16 November, the areal-mean w at 1547 m is in fact slightly negative (figure not
shown) and indicates leeside sinking and stretching (Fig. 9a). After 0600 UTC 17 November,
on the other hand, mean w turns positive with growth in ζ near 1 km (Fig. 8a), as the vortex
gradually moves away from the terrain (cf. Fig. 6a). While the budget results exhibit similar
characteristics in the NT run (Fig. 9b), the convergence and vertical advection terms are often
smaller than in CTL, yielding a mean ζ (at 1547 m) of roughly 1.4×10^{-5} s ⁻¹ at 0000 UTC 18
November. On 17 November when the mean ζ starts to show larger deficit (cf. Fig. 8c), such
differences in budget terms are also more evident. The increase in both the convergence and
vertical advection terms in CTL on 17 November indicate that the two effects work in phase.
In short, the results from Figs. 8 and 9 suggest that the Sumatra topography is helpful to
produce a stronger pre-Nisha vortex at the leeside, and most likely as a result, Nisha reaches
the TS status 27 h earlier in CTL compared to its counterpart in NT.
As reviewed in section 1, the blocking effect of Sumatra on the northeasterly flow can be
characterized by Fr , and a larger (smaller) value favors the flow-over (flow-around) regime.
Here, h is set to 1895 m obtained for northern Sumatra, and the mean U and N values (time
variant) at 3°-7°N along 100°E below 2 km (cf. Fig. 1a) are used following Fine et al. (2016).
To reveal possible influence of Fr on vorticity generation at the leeside, the correlation
coefficients between Fr and lagged mean vorticity tendency at 1547 m (as in Fig. 9) from
hourly data are computed and presented in Fig. 10a for the pre-Nisha vortex. In CTL, the
coefficient (green curve) is positive and at least ~0.2 for all lag time within 24 h, but is higher

over 18-24 h with a peak value of 0.46. While these values are not high (since Fr is only one of the factors), this result indicates that a strengthening in the low-level prevailing northeasterly flow generally helps to increase the leeside vorticity, and its influence is quite persistent. Without the terrain in NT (U and N are different from those in CTL, but h is still set to 1895 m for consistency), on the other hand, the enhancement in northeasterly flow can contribute more directly to the lee vortex, as the coefficient peaks at 0.69 at a lag time of only 3 h and remains >0.5 within 7 h. However, the coefficient drops rapidly after 11 h (Fig. 10a), so the influence does not last long.

379 b. Tropical Storm Ward (2009)

371

372

373

374

375

376

377

378

380

381

382

383

384

385

386

387

388

389

390

391

392

393

394

395

For TS Ward (2009), the observed and modeled track and intensity are presented in Fig. 11. All four tracks (JTWC, ECMWF-YOTC, and the two model runs CTL and NT) are close to one another, with movement generally toward the west during 3-9 December and then toward the north during 9-12 December afterwards (Fig. 11a). As in JTWC, the storms eventually make landfall in central Sri Lanka from the east, though with some variations in timing. The landfall time in ECMWF data is near 1800 UTC 12 December and about 40 h earlier than that in JTWC (1200 UTC 14 December), and a similar early landfall also occurs in the two CReSS experiments, near 1500 UTC in CTL and 1800 UTC in NT on 12 December. Again, at a range of nearly two weeks, such track errors (about 200 km) in Fig. 11a are in fact very small. Before landfall, all four data give almost identical timing, within a 6-h period, to reach the TS status on 11 December (Fig. 11b). The two simulations produce a maximum surface wind speed stronger than JTWC best-track, but the intensity quickly drops after 12 December (especially in CTL) due to the early landfall. Most likely for the same reason, the central MSLP in the model runs over 12-13 December are also not as low as that in JTWC (Fig. 11c), as they are closer to Sri Lanka than the observation. During 6-9 December when the pre-Ward vortex tracks westward, nevertheless, its intensity in CTL tends

to be stronger compared to NT (Fig. 11b).

396

397

398

399

400

401

402

403

404

405

406

407

408

409

410

411

412

413

414

415

416

417

418

419

420

For the period since 6 December, the storm rainfall structure and low-level circulation of Ward in CTL are compared with SSMI satellite observation and YOTC data in Fig. 12. Similar to the Nisha case, the model successfully captures the general characteristics of rainfall structure, its asymmetry, and time evolution. As the storm tracked toward Sri Lanka in the NIO on 6 December, the convection was loose and farther away from the center (Figs. 12a,d). During 9-12 December as the storm strengthened to reach TS (cf. Fig. 11b), it became tighter in cloud structure (Figs. 12b,e), and developed in a clear comma cloud shape to the east of the storm center on 11-12 December (Figs. 12c,f). However, this structure deteriorated afterwards as the storm moved closer to land (not shown). The time-height plot of areal-mean ζ inside the radius of 550 km in CTL for the vortex in the case of Ward, as shown in Fig. 13a, agree reasonably well with that constructed from ECMWF-YOTC analyses (cf. Fig. 2d), and both are weaker and do not extend upward as deep compared to the Nisha case (cf. Figs. 2b and 8a). Again, the time-height structure of ζ in NT (Fig. 13b) is very close to CTL, and there is a tendency for downward development of ζ in the lee stage in both runs, from about 5 km toward the lower levels. While close, Fig. 13c still reveals that the vortex in CTL is stronger than that in NT during most of the lee stage that ends at 0000 UTC 4 December, except for a brief period around 0000 UTC 3 December. This difference in lee vortex strength is more pronounced than the Nisha case (cf. Fig. 8c). However, such an advantage of CTL over NT does not maintain throughout the life span of Ward, and the storm in CTL reaches TS intensity only 4 h earlier (Fig. 11b). The areal-mean vorticity budget (550 km from center) at 1547 m for the pre-Ward lee vortex (t = 24-96 h) in CTL (Fig. 14a) shows that the mean ζ is generally above 1.2×10^{-5} s⁻¹ from 1800 UTC 30 November to 1200 UTC 2 December and mainly contributed by the

convergence/stretching term (green), which is again largely cancelled by horizontal advection.

In this case, the vertical advection term (brown) can be either positive or negative in different
time periods but remains out of phase from the tilting effect (red), which therefore also
contributes toward ζ from time to time (when negative vertical advection occurs). In periods
when the areal-mean w at 1547 m is negative (e.g., first half on 1 December, not shown), this
leeside sinking (with downward acceleration) is accompanied by positive convergence and
vertical stretching effect (Fig. 14a). In NT, the ζ -budget calculation reveals similar results to
CTL (Fig. 14b), but the contribution from convergence is generally smaller and the mean ζ
grows to exceed $1.2 \times 10^{-5} \text{ s}^{-1}$ only toward the end, after about 1200 UTC 2 December. This
is because a BV (visible in Figs. 3d, 4d, and 5d) is moving across the northern Sumatra (near
97°E) from upstream around this time, and without Sumatra's terrain, the lee vortex in NT
moves eastward to merge with the BV (Fig. 11a), resulting in an increase in mean ζ and a
stronger vortex in NT (versus CTL) near 3 December (Fig. 14). In contrast, with topography,
the lee vortex in CTL remains stationary near 3 December, and a direct merger does not occur
(Fig. 11a).

The results of lagged correlation between upstream Fr and areal-mean ζ at 1547 m at the leeside (east of 90°E and before 0600 UTC 2 December to exclude the influence from the BV) indicate that for the pre-Ward lee vortex, the coefficient (green) in CTL remains high within about 10 h and peaks at 0.54 with a 5-h lag time (Fig. 10b). In contrast, the coefficient drops rapidly after only 3 h in NT, from a maximum of 0.47 at 1 h. Thus, in both Nisha and Ward, the terrain tends to exert a longer, more persistent influence on the generation of leeside vorticity (through either subsidence warming or corner effect, or both) in CTL experiments, in comparison to NT runs where ζ is provided only through horizontal advection and/or shearing effect and for a shorter duration.

5. Model results of Cleo in the southern Indian Ocean

During the same period as Ward, another vortex also evolved into Cyclone Cleo in SIO
as mentioned, so the same simulations (CTL and NT) are used to discuss its development as
well here. Since the equatorial westerlies were present leading to the formation of this closed
vortex to the west of southern Sumatra/western Java (Fig. 3d), the pre-Cleo vortex is not a lee
vortex as pointed out by Fine et al. (2016). After formation, pre-Cleo first remained stationary
for a few days, then moved toward the west-southwest quite steadily after 3 December (Fig.
15a). In CTL and NT, the corresponding vortices both form at the same location and time (at
0000 UTC 29 November) as the YOTC analysis, and also have a similar track. However,
compared to analysis, the vortex in CTL starts to move westward (near 0600 UTC 3
December) about 12-18 h too late, and even more so in NT (Fig. 15a). Later in the simulations
after 1200 UTC 8 December, all tracks converge toward the JTWC with reduced track errors.
The JTWC best-track data indicate that Cleo reached TS intensity near 0000 UTC 7
December (Fig. 15b) but this occurs roughly 24 h later in CTL, and another 12 h later in NT,
whose vortex moves out from its formation area the latest, as mentioned. Both vortices,
nonetheless, reach 34 kts at an earlier time but only briefly. After 1200 UTC 7 December, TC
Cleo underwent a period of rapid intensification to reach a peak wind speed of over 110 kts
and a central MSLP of lower than 940 hPa (Figs. 15b,c). In the model, however, the storm is
gradually approaching the domain boundary during this period (cf. Fig. 1b) and a similar
intensification does not take place. Although not ideal, this is acceptable since our focus is on
the formation and earlier stages of the vortex. For selected times during 3-7 December, Cleo's
rainfall structure in CTL is also compared with satellite observations, and the two are similar
and in good agreement, including the asymmetry and evolutionary characteristics (Fig. 16).
The time-height cross sections of areal-mean ζ (inside 550 km) of the pre-Cleo vortex
are again similar in CTL and NT runs (Fig. 17), where a downward development of ζ with
time is evident before 5 December. In Fig. 17c, one can also see that the vortex in CTL is

persistently stronger and extends deeper into the upper troposphere than that in NT during the stationary stage closer to Sumatra, but not so at low levels after 4-5 December. This latter difference, however, mainly exists only over outer regions at larger radii, as the peak 10-m wind at the inner core remains clearly stronger in CTL over 5-8 December (cf. Fig. 15b).

Prior to 0000 UTC 4 December (*t* = 48-120 h), the generation of mean vorticity is again mainly from convergence/stretching and vertical advection terms (Fig. 18), which also tend to be greater in CTL than those in NT. In Fig. 19, the low-level mean winds below 2 km over the northeastern quadrant of the vortex (also within 550 km) in the two experiments are compared. Without the topography, the mean wind is between westerly and west-northwesterly in NT, but persistently northwesterly in CTL. Thus, the Sumatra Island acts to block the equatorial westerly flow to provide a larger southward component and stronger curvature vorticity at low levels. This result is consistent with Fine et al. (2016), who speculated that the topography of Sumatra helps the vortex of pre-Cleo to gain strength. Thus, in the case of Cleo (2009) where its initial vortex is not at the leeside, the blocking effect of southern Sumatra on the equatorial westerlies, nevertheless, helps to provide stronger curvature vorticity and leads to a stronger, tighter and more compact vortex during it westward movement. Eventually, the storm in CTL reaches the TS status 12 h before that in NT (Fig. 15b).

6. Discussion

In the CTL experiments, the two lee vortices in NIO (Nisha and Ward) tend to be stronger during the majority of the lee stage (Figs. 8 and 13) and subsequently reach the TS status earlier compared to their counterpart in NT runs (Fig. 6b), although the difference is small and perhaps not significant for Ward (Fig. 11b). Despite this, however, the storms in NT runs form in approximately the same location and reach TS status (although more slowly)

without the topography of Sumatra. Even if a different criterion for TC formation, 25 kts for
example, is adopted, the results are similar (cf. Figs. 6b and 11b). Thus, for the cases
simulated here, our results indicate that the island of Sumatra is only a beneficial factor rather
than a necessary condition for the formation of TCs (typically several days later). This
conclusion should not come as a surprise since the majority of named TCs in NIO do not
originate from the leeside of Sumatra (e.g., Fine et al., 2016). It follows that some other
factors common in both CTL and NT runs must play a more determinant role in the
subsequent evolution and intensification of the vortex after vortex shedding. It is known that
both a stronger initial vortex and favorable synoptic evolution surrounding it are important to
TC genesis (section 1), in addition to mesoscale convection and non-linear interactions. In
section 3, low-level northeasterly winds across or near northern Sumatra, equatorial WWBs at
low latitudes, and advection of vorticity and/or moisture from upstream into the lee area are
seen to be the common ingredients in all four cases of 03A, Nisha, 07B, and Ward (Figs. 3-5).
To find out how frequently these conditions/features occur for the TCs, here we use the
ECMWF-YOTC data to check their occurrence in all 22 vortices in the tropical NIO that
appeared west of 90°E and possessed closed circulation for at least 24 h at 925 hPa during
October-December in 2008 and 2009 (including those not tied to Sumatra) following the same
procedure as in section 3. The overall results are presented in Fig. 20.
In Fig. 20, the time series of equatorial westerly wind speed (averaged also over 5°S-
5°N, 80°-90°E) and northeasterly wind speed (averaged over 5°-10°N, 107°-115°E), both at
925 hPa, are shown together with the periods with storms tracked by JTWC and those with
vorticity (pink) and/or water vapor advection (orange) at 700 hPa (above Sumatra's terrain).
While the low-level northeasterly winds generally strengthen from October to December and
the equatorial westerly winds tend to be stronger in November, both of them are characterized
by surges or pulses. During their early stage, the majority of vortices were associated with

simultaneous surges in both northeasterly flow near northern Sumatra and equatorial westerly
flow (Fig. 20). Among the seven cases that reached TS, the only exception is Phyan (2009),
where the equatorial westerly was weak and only 2-3 m $\rm s^{-1}$ (Fig. 20b). During the formation
stage, many disturbances were also accompanied by either vorticity or moisture advection, or
both, especially in the Bay of Bengal (BOB) where many vortices originated from the leeside
of Sumatra. Thus, not only in the four cases in section 3 (Figs. 2-5), the low-level
environment that provided a background of cyclonic wind shear and the advection of
vorticity/moisture from upstream into the area of initial vortex were also common features in
nearly all cases in October-December of 2008 and 2009. Thus, these synoptic features are
undoubtedly important factors for the development of initial vortices toward the TS/TC status
in the NIO. Due to these favorable factors (and a positive interaction with the convection) in
the cases of Nisha and Ward, a similar vortex can still develop to reach TS status even in the
NT runs when Sumatra's topography is removed in the model. In eastern Pacific, an
analogous situation exists, as many easterly wave disturbances there can be traced back to
those from the North Atlantic crossing Central America (Rydbeck et al. 2017).
Based on the findings in this study, a modified conceptual model from Kuettner (1967,
1989; Fig. 1a) is presented below in Fig. 21. In the NIO, the northeasterly wind (from
upstream across the Malaysia Peninsula) near the northern tip of Sumatra combines with the
equatorial westerly wind surge to provide a favorable background shear for the lee vortex to
evolve. Frequently, the lee vortices are maintained and enhanced by incipient disturbances (a
BV or TC/TS remnant) from the SCS, in the form of vorticity and/or moisture advection into
the leeside. In these cases, the topography of Sumatra can provide additional help through
flow deflection and lee cyclogenesis to further enhance the vorticity during the lee stage, but
it is not a necessary factor. For SIO, Cleo (2009) is the only storm studied herein. In this case,
the northeasterly wind did not reach the southern latitudes, and southwestern Sumatra is on

the windward side instead of leeside due to the equatorial westerly wind. However, Sumatra played a role to deflect the westerly wind southward and provide a larger vorticity together with the southeasterly trade wind farther south. Thus, the hypothesis of Fine et al. (2016) is confirmed and the topography is also helpful for TC formation, and the synoptic conditions remain favorable for dual-vortex formation across the equator (as in the case of Ward and Cleo). In contrast to the original model proposed by Kuettner (1967, 1989) in Fig. 1a, our conceptual model (Fig. 21) also includes the roles of equatorial westerly wind and upstream incipient disturbances from the SCS, with a different formation scenario for the vortex in SIO, namely, not at the leeside of topography.

7. Summary and conclusion

Building upon the observational study of Fine et al. (2016), the present work has selected a few of their cases for more detailed analysis and three cases for high-resolution numerical simulation and sensitivity test to investigate the role played by the island of Sumatra in subsequent TC formation in the IO. The CReSS model employed has a convective-permitting 4-km grid size and large domain of $5600 \times 4464 \text{ km}^2$ (Table 1), and the simulations for the three cases, including Nisha (2008) in NIO and the TC pairs of Ward and Cleo (2009), are for at least 15 days. In the CTL runs, the evolution of the vortices, including the lee stage (for Nisha and Ward), is reasonably well-captured. The results are then compared and contrasted to those in the sensitivity tests (NT runs), in which the topography of Sumatra is removed. The major findings of the present study can be summarized below.

1. In the NT tests without Sumatra topography, the three TC cases initiate in approximately the same location and also all reach TS status as in the CTL experiment and observation, but tend to do so at a later time. This time difference is 27 h for Nisha (2008), 12 h for Cleo (2009), and only 4 h for Ward (2009). The island of Sumatra therefore is not a

- necessary condition for TC genesis in the IO, as expected.
- 572 2. During the leeside stage of Nisha and Ward in NIO, both vortices in the CTL runs tend to
- possess a slightly stronger areal-mean vorticity in the low level compared to their
- counterpart in NT runs. A vorticity budget analysis indicates that the main contributing
- terms are vertical stretching and vertical advection at the leeside. Thus, the Sumatra
- topography appears helpful in producing a larger vorticity and stronger initial vortex for
- subsequent development after vortex shedding.
- 578 3. For the four NIO cases examined, easterly or northeasterly winds near the northern tip of
- Sumatra, equatorial westerly wind surge, and advection of vorticity and moisture from
- upstream (either a TC/TS remnant or a BV) are common synoptic features at (or near)
- the formation of the lee vortex. A more extensive examination of 22 vortices in October-
- December of 2008 and 2009 suggests that these favorable factors were also frequently
- present, especially in those that reached TS status in the BOB. Evidently, with these
- features and their associated environment, the convection and non-linear interactions
- lead to the intensification of the vortex in NT runs, often from a (slightly) weaker vortex
- without Sumatra topography.
- 587 4. For Cleo (2009) in SIO, the formation area is not at lee but windward side due to the
- presence of equatorial westerly wind surge, as analyzed by Fine et al. (2016). The
- Sumatra topography in this case has a deflection effect on the westerly, and thereby
- provides stronger vorticity (in combination with southeasterly wind farther south).
- Subsequently, the inner vortex in CTL remains stronger and reaches TS status earlier
- than its counterpart in the NT experiment.
- 593 5. A conceptual model is presented in Fig. 21, which summarizes the above results and
- depicts the favorable conditions for TC genesis in NIO from initial vortex from the
- leeside of Sumatra as well as SIO. For NIO, these include northeasterly wind near 5°-

596	10°N, equatorial WWB, and advection of vorticity/moisture from SCS. For SIO cases,
597	they include the southward flow deflection of westerlies and southeasterly trade wind at
598	higher latitudes.
599	The simulation results of Nisha (2008) and Ward (2009) and the conceptual model
600	obtained here are likely applicable to many TCs in the NIO that originate from the lee of
601	Sumatra, but presumably not all of them. More high-resolution simulations are recommended
602	in the future to further explore the potential role played by the Sumatra topography on TC
603	formation, including those in the SIO. An ensemble approach is also recommended to
604	adequately address the uncertainty issue in deterministic simulations of chaotic systems, i.e.,
605	to properly isolate the differences caused by the topography from those arising from
606	nonlinearity.
607	
608	Acknowledgements. The authors wish to thank the four anonymous reviewers, as well as Prof.
609	CS. Lee of the National Taiwan University, for their helpful comments that lead to
610	significant improvement of the manuscript. The ECMWF and YOTC project is acknowledged
611	for making available the gridded analysis data. The TRMM PR/TMI observations in Figs. 7,
612	12, and 16 are provided by the NRL, and Ms. Shin-Yi Huang also helped with the plotting.
613	This study is jointly supported by the Ministry of Science and Technology (MOST) of Taiwan
614	under Grants MOST-105-2111-M-003-003-MY3, MOST-108-2111-M-003-005-MY2, and
615	MOST-108-2625-M-003-001. Richard Johnson acknowledges support under National Science
616	Foundation (NSF) under Grants AGS-1360237 and AGS-1853633.
617	

618 References

- 619 Chang, C.-P., C.-H. Liu and H.-C. Kuo, 2003: Typhoon Vamei: An equatorial tropical cyclone
- 620 formation. *Geophys. Res. Lett.*, **30**, No. 3, 1150.
- 621 Chang, C.-P., P. A. Harr, and H. J. Chen, 2004: Synoptic disturbances over the equatorial
- South China Sea and western maritime continent during boreal winter. *Mon. Wea. Rev.*,
- 623 **133**, 489–503.
- 624 Charney, J. G., and A. Eliassen, 1964: On the growth of the hurricane depression. *J. Atmos.*
- 625 *Sci.*, **21**, 68–75.
- 626 Chen, Y.-H., H.-C. Kuo, C.-C. Wang, and Y.-T. Yang, 2017: Influence of southwest monsoon
- flow and typhoon track on Taiwan rainfall during the exit phase: Modeling study of
- 628 Typhoon Morakot (2009). Quart. J. Roy. Meteor. Soc., 143 (B), 3014–3024, doi:
- 629 10.1002/qj.3156.
- 630 Cotton, W. R., G. J. Tripoli, R. M. Rauber, and E. A. Mulvihill, 1986: Numerical simulation of
- the effects of varying ice crystal nucleation rates and aggregation processes on
- orographic snowfall. J. Climate Appl. Meteor., 25, 1658–1680.
- 633 Deardorff, J. W., 1980: Stratocumulus-capped mixed layers derived from a three-dimensional
- 634 model. *Bound.-Layer Meteor.*, **18**, 495–527.
- Emanuel, K. A., 1986: An air-sea interaction theory for tropical cyclones. Part I: Steady-state
- 636 maintenance. J. Atmos. Sci., 43, 585–604.
- Epifanio, C. C., 2003: Lee vortices. *Encyclopedia of Atmospheric Sciences*, J. R. Holton, J.
- Pyle, and J. A. Curry, Eds., Elsevier Science Ltd., 1150–1160.
- 639 Farfán, L. M., and J. A. Zehnder, 1997: Orographic influence on the synoptic-scale
- circulations associated with the genesis of Hurricane Guillermo (1991). Mon. Wea. Rev.,
- **125**, 2683–2698.
- Fine, C. M., R. H. Johnson, P. E. Ciesielski, and R. K. Taft, 2016: The role of topographically

- induced vortices in tropical cyclone formation over the Indian Ocean. Mon. Wea. Rev.,
- **127**, 4827–4847.
- 645 Gray, W. M., 1968: Global view of the origins of tropical disturbances and storms. *Mon. Wea.*
- 646 *Rev.*, **96**, 669–700.
- Ikawa, M., and K. Saito, 1991: Description of a nonhydrostatic model developed at the
- Forecast Research Department of the MRI. MRI Tech. Rep. 28, 238 pp.
- Johnson, R. H., and P. E. Ciesielski, 2013: Structure and properties of Madden–Julian
- oscillations deduced from DYNAMO sounding arrays. J. Atmos. Sci., 70, 3157–3179,
- doi:10.1175/JAS-D-13-065.1.
- Kikuchi, K., and B. Wang, 2010: Formation of tropical cyclones in the northern Indian Ocean
- associated with two types of tropical intraseasonal oscillation modes. *J. Meteor. Soc.*
- 654 *Japan*, **88**, 475–196.
- Kondo, J., 1976: Heat balance of the China Sea during the air mass transformation
- 656 experiment. J. Meteor. Soc. Japan, **54**, 382–398.
- Kuettner, J. P., 1967: The equatorial double vortex: Unique hydrodynamic role of Sumatra in
- atmospheric developments over the Indian Ocean. Bull. Amer. Meteor. Soc., 48, 637.
- Kuettner, J. P., 1989: Easterly flow over the cross equatorial island of Sumatra and its role in
- the formation of cyclone pairs over the Indian Ocean. *Wetter Leben*, **4**, 47–55.
- Kuo, H.-C., S. Tsujino, C.-C. Huang, C.-C. Wang, and K. Tsuboki, 2019: Diagnosis of the
- dynamic efficiency of latent heat release and the rapid intensification of Supertyphoon
- Haiyan (2013). *Mon. Wea. Rev.*, **147**, 1127–1147, doi: 10.1175/MWR-D-18-0149.1.
- 664 Lee, C.-S., 1986: An observational study of tropical cloud cluster evolution and cyclogenesis
- in the western North Pacific. Dept. of Atmos. Sci. Paper No. 403, Colo. State Univ., Ft.
- 666 Collins, CO, 250 pp.
- Lee, C.-S., R. Edson, and W. M. Gray, 1989: Some large-scale characteristics associated with

- tropical cyclone development in the North Indian Ocean during FGGE. Mon. Wea. Rev.,
- 669 **117**, 407–426.
- 670 Lin, Y.-L., and C.-S. Lee, 2011: An analysis of tropical cyclone formations in the South China
- 671 Sea during the late season. *Mon. Wea. Rev.*, **139**, 2748–2760.
- 672 Lin, Y.-L., R. D. Farley, and H. D. Orville, 1983: Bulk parameterization of the snow field in a
- 673 cloud model. *J. Climate Appl. Meteor.*, **22**, 1065–1092.
- 674 Louis, J. F., M. Tiedtke, and J. F. Geleyn, 1982: A short history of the operational PBL
- parameterization at ECMWF. Workshop on Planetary Boundary Layer Parameterization,
- 676 25-27 November 1981, Reading, UK, 59–79.
- 677 Love, G., 1985a: Cross-equatorial influence of winter hemisphere subtropical cold surges.
- 678 *Mon. Wea. Rev.*, **113**, 1487–1498.
- 679 Love, G., 1985b: Cross-equatorial interaction during tropical cyclone genesis. *Mon. Wea.*
- 680 *Rev.*, **113**, 1499–1509.
- Moncrieff, M. W., D. E. Waliser, M. J. Miller, M. A. Shapiro, G. R. Asrar, and J. Caughey,
- 682 2012: Multiscale convective organization and the YOTC virtual global field campaign.
- 683 Bull. Amer. Meteor. Soc., 93, 1171–1187, doi:10.1175/BAMS-D-11-00233.1.
- Mozer, J. B., and J. A. Zehnder, 1996: Lee vorticity production by large-scale tropical
- mountain ranges. Part I: A mechanism for tropical cyclogenesis in the eastern North
- 686 Pacific. J. Atmos. Sci., **53**, 521–538.
- Murakami, M., 1990: Numerical modeling of dynamical and microphysical evolution of an
- isolated convective cloud---The 19 July 1981 CCOPE cloud. J. Meteor. Soc. Japan, 68,
- 689 107–128.
- Murakami, M., T. L. Clark, and W. D. Hall, 1994: Numerical simulations of convective snow
- clouds over the Sea of Japan: Two-dimensional simulation of mixed layer development
- and convective snow cloud formation. J. Meteor. Soc. Japan, 72, 43–62.

- 693 Ooyama, K. V., 1982: Conceptual evolution of the theory and modeling of the tropical
- 694 cyclone. *J. Meteor. Soc. Japan*, **60**, 369–379.
- Ritchie, E. A., and G. J. Holland, 1999: Large-scale patterns associated with tropical
- 696 cyclogenesis in the western Pacific. *Mon. Wea. Rev.*, **127**, 2027–2043.
- Rotunno, R., and K. A. Emanuel, 1987: An air-sea interaction theory for tropical cyclones.
- Part II: Evolutionary study using a nonhydrostatic axisymmetric numerical model. J.
- 699 Atmos. Sci., 44, 542–561.
- Rotunno, R., and P. K., Smolarkiewicz, 1991: Further results on lee vortices in low-Froude-
- 701 number flow. *J. Atmos. Sci.*, **48**, 2204–2211.
- Rydbeck, A. V., E. C. Maloney, and G. J. Alaka, Jr., 2017: In situ initiation of East Pacific
- easterly waves in a regional model. *J. Atmos. Sci.*, **74**, 333–351.
- Segami, A., K. Kurihara, H. Nakamura, M. Ueno, I. Takano, and Y. Tatsumi, 1989:
- Operational mesoscale weather prediction with Japan Spectral Model. *J. Meteor. Soc.*
- 706 Japan, **64**, 637–664.
- Subbaramayya, I., and S. R. M. Rao, 1984: Frequency of Bay of Bengal cyclones in the post-
- 708 monsoon season. *Mon. Wea. Rev.*, **112**, 1640–1642.
- 709 Smolarkiewicz, P. K., and R. Rotunno, 1989: Low Froude number flow past three-
- dimensional obstacles. Part I: Baroclinically generated lee vortices. J. Atmos. Sci., 46,
- 711 1154–1164.
- 712 Takahashi, H. G., Y. Fukutomi, and J. Matsumoto, 2011: The impact of long-lasting northerly
- surges of the East Asian winter monsoon on tropical cyclogenesis and its seasonal march.
- 714 *J. Meteor. Soc. Japan*, **89A**, 181–200.
- 715 Tsuboki, K., and A. Sakakibara, 2002: Large-scale parallel computing of cloud resolving
- storm simulator. *High Performance Computing*, Springer, H. P. Zima et al. Eds., 243–
- 717 259.

- 718 Tsuboki, K., and A. Sakakibara, 2007: Numerical Prediction of High-Impact Weather Systems.
- 719 The Textbook for the Seventeenth IHP Training Course in 2007. Hydrospheric
- Atmospheric Research Center, Nagoya University and UNESCO, 273 pp.
- Waliser, D. E., and Coauthors, 2012: The "Year" of Tropical Convection (May 2008–April
- 722 2010): Climate variability and weather highlights. Bull. Amer. Meteor. Soc., 93, 1189–
- 723 1218, doi:10.1175/2011BAMS3095.1.
- Wang, C.-C., 2015: The more rain, the better the model performs—The dependency of
- quantitative precipitation forecast skill on rainfall amount for typhoons in Taiwan. *Mon.*
- 726 Wea. Rev., 143, 1723–1748, doi:10.1175/MWR-D-14-00137.1.
- 727 Wang, C.-C., H.-C. Kuo, Y.-H. Chen, H.-L. Huang, C.-H. Chung, and K. Tsuboki, 2012:
- Effects of asymmetric latent heating on typhoon movement crossing Taiwan: The case of
- 729 Morakot (2009) with extreme rainfall. *J. Atmos. Sci.*, **69**, 3172–3196.
- Wang, C.-C., Y.-H. Chen, H.-C. Kuo, and S.-Y. Huang, 2013: Sensitivity of typhoon track to
- asymmetric latent heating/rainfall induced by Taiwan topography: A numerical study of
- 732 Typhoon Fanapi (2010). J. Geophys. Res., 118(D8), 3292–3308, doi:10.1002/jgrd.50351.
- 733 Wang, C.-C., H.-C. Kuo, R. H. Johnson, C.-Y. Lee, S.-Y. Huang, and Y.-H. Chen, 2015: A
- numerical study of convection in rainbands of Typhoon Morakot (2009) with extreme
- rainfall: Roles of pressure perturbations with low-level wind maxima. *Atmos. Chem.*
- 736 *Phys.*, **15**, 11097–11115, doi:10.5194/acp-15-11097-2015.
- Wang, C.-C., S.-Y. Huang, S.-H. Chen, C.-S. Chang, and K. Tsuboki, 2016: Cloud-resolving
- typhoon rainfall ensemble forecasts for Taiwan with large domain and extended range
- through time-lagged approach. Wea. Forecasting, **31**, 151–172.
- Zehnder, J. A., D. M. Powell, and D. L. Ropp, 1999: The interaction of easterly waves,
- orography, and the intertropical convergence zone in the genesis of eastern Pacific
- 742 tropical cyclones. *Mon. Wea. Rev.*, **127**, 1566–1585.

Figure caption

745	FIG. 1. (a) The topography of Sumatra and surrounding region (m, color), and a schematic of
746	lee vortices based on Kuettner (1967). The gray-dotted polygon shows the area to
747	remove terrain in sensitivity tests, and the red-dotted line shows the segment used to
748	compute Fr. (b) Tracks of the five selected cases (thickened for lifespan reaching TS
749	intensity) and the model simulation domain (thick solid box).
750	FIG. 2. Time-height section of mean relative vorticity (ζ , 10^{-6} s ⁻¹), computed from ECMWF-
751	YOTC data and averaged inside 550 km from the vortex center, for the four cases in
752	NIO: (a) 03A, (b) Nisha, (c) 07B, and (d) Ward. Each panel starts at the time of lee
753	vortex formation. The thick dashed vertical lines mark the time when the vortex started
754	to move downstream and the arrows denote when the TS intensity is reached in JTWC
755	best-track data (not applicable for 03A). The gray dashed horizontal lines depict the level
756	of maximum vorticity.
757	FIG. 3. Distributions of horizontal wind (gray vectors, m $\rm s^{-1}$) and relative vorticity ($10^{-5} \rm s^{-1}$,
758	color, cyclonic only) in ECMWF-YOTC data two days before (left), at the time (middle)
759	of, and two days after (right) the formation of the lee vortex for (a) 03A at 850 hPa, (b)
760	Nisha at 700 hPa, (c) 07B at 500 hPa, and (d) Ward at 600 hPa. Both the reference vector
761	and color scales are plotted at the bottom. The vortex centers at 850 hPa are marked by a
762	green "x" [not necessarily the same as the center at the level shown in (b)-(d)].
763	FIG. 4. Longitude-time (Hovmoller) diagrams of mean (a)-(d) relative vorticity (10^{-5} s^{-1}) at
764	the pressure level as labeled (same as in Fig. 3) and (e)-(h) total column-integrated
765	precipitable water (mm) in ECMWF-YOTC data during the case period of 03A, Nisha,
766	07B, and Ward, respectively (from top to bottom). The latitudinal range of averaging is
767	0°-15°N. The circles depict the time of lee vortex formation, a disturbance is depicted as
768	"DB", and the vertical dashed lines near 100°E mark the boundary between the IO and

- the SCS.
- FIG. 5. Distribution of total column-integrated precipitable water (mm, color) and horizontal
- wind at 925 hPa (m s⁻¹, gray vectors) at the time of lee vortex formation for (a) 03A, (b)
- Nisha, (c) 07B, and (d) Ward, respectively. The vortex centers (at 850 hPa) are marked
- by an "x". The red dashed circles depict TC or disturbance (DB) in the IO, green dashed
- circles depict TD or pre-TC in SIO, and white dashed circles depict BV or TC remnant in
- the SCS. Both the reference vector and color scales are plotted at the bottom.
- FIG. 6. Comparison of (a) track, (b) maximum surface wind speed (kts, at 10 m above the
- surface), and (c) central mean sea-level pressure (hPa) among JTWC best track,
- ECMWF-YOTC, and CTL and NT experiments for the case of Nisha (16 to 28 Nov
- 779 2008). The vortex center positions (at or near 850 hPa) are given by small dots every 6 h,
- median dots at 0000 UTC, and large dots every three days with dates labeled (unless not
- necessary) in (a). Track endpoints are also labeled (with time if not at 0000 UTC). In (b),
- TS intensity (34 kts) and the time to reach it in the four data sources are marked.
- FIG. 7. (a)-(d) SSMI 91-GHz imagery of brightness temperature (T_B , K, color) of Nisha at (a)
- 784 0151 UTC 23, (b) 1154 UTC 24, (c) 0021 UTC 26, and (d) 0008 UTC 27 Nov 2008
- 785 (source: NRL), overlaid with ECMWF-YOTC wind fields (kts, 1 full barb = 10 kts) at
- 786 850 hPa at the closest time with data (every 6 h). (e)-(h) Column maximum mixing ratio
- of precipition (g kg $^{-1}$, rain + snow + graupel) and horizontal wind at 1547 m (kts) in CTL
- 788 at (e) 2000 UTC 22, (f) 1500 UTC 24, (g) 2300 UTC 25, and (h) 0900 UTC 27 Nov,
- respectively. The color scales are plotted at the bottom, and the storm center is marked
- 790 by an "x".
- FIG. 8. Time-height section of mean relative vorticity (ζ , 10^{-6} s⁻¹) for Nisha similar to Fig.
- 2b, except from (a) CTL and (b) NT experiment, and (c) their difference (CTL NT).
- Downward developments during the lee stage are marked.

- FIG. 9. The vorticity-tendency budget terms (10^{-9} s⁻², left axis), including local tendency,
- horizontal advection, vertical advection, convergence, tilting, solenoidal, and residual
- terms (see legend), and the mean vorticity (10^{-5} s⁻¹, dashed with dots, right axis) at the
- height of 1547 m, averaged inside 550 km, for Nisha from 1200 UTC 15 Nov to 0000
- 798 UTC 18 Nov 2008 in (a) CTL and (b) NT experiment.
- FIG. 10. The correlation coefficients between Fr and lagged mean vorticity tendency (as in
- Figs. 9 and 14), as a function of lagged time (h) in CTL and NT experiments for the case
- of (a) Nisha and (b) Ward, respectively.
- FIG. 11. As in Fig. 6, except for the case of TC Ward (30 Nov to 16 Dec 2009).
- 803 FIG. 12. As in Fig. 7, except for Ward at (a) 1130 UTC 6, (b) 2334 UTC 9, and 0146 UTC 12
- Dec 2009 (source of satellite imagery: NRL), and (d) 1200 UTC 6, (e) 2100 UTC 9, and
- (f) 1400 UTC 12 Dec from CTL at a similar stage as in (a)-(c), respectively.
- FIG. 13. As in Fig. 8, except for the case of TC Ward.
- 807 FIG. 14. As in Fig. 9, except for Ward from 0000 UTC 30 Nov to 0000 UTC 3 Dec 2009.
- FIG. 15. As in Fig. 6, except for the case of TC Cleo (29 Nov to 10 Dec 2009).
- 809 FIG. 16. As in Fig. 7, except for Cleo at (a) 1302 UTC 3, (b) 1139 UTC 5, and (c) 1353 UTC
- 7 Dec 2009 (source of satellite imagery: NRL), and (d) 2200 UTC 3, (e) 1900 UTC 5,
- and (f) 2000 UTC 7 Dec from CTL at a similar stage as in (a)-(c), respectively. The
- storm center in (c) is not marked for clarity.
- FIG. 17. As in Fig. 8, except for the case of TC Cleo.
- 814 FIG. 18. As in Fig. 9, except for Cleo from 0000 UTC 1 Dec to 0000 UTC 4 Dec 2009. Note
- that the vertical scale is reversed for this case in the Southern Hemisphere.
- 816 FIG. 19. Averaged low-level horizontal wind (m s⁻¹, over 50-1913 m) in the northeastern
- guadrant of Cleo at 1-h intervals from 0000 UTC 1 Dec to 0000 UTC 4 Dec 2009 in
- 818 CTL and NT experiments.

819	FIG. 20. Time-series of westerly wind speed in equatorial IO (kts, red, averaged over 5°S-		
820	5°N, 80°-90°E) and northeasterly wind speed east of northern Sumatra (kts, blue,		
821	averaged over 5°-10°N, 107°-115°E) at 925 hPa in the ECMWF-YOTC data during Oct-		
822	Dec of (a) 2008 and (b) 2009. Black/gray segments indicate periods with a closed vortex		
823	in BOB/Arabian Sea (divided at 80°E) with named storms labeled (the naming times		
824	shown by short red ticks). The periods with 700-hPa positive vorticity advection (pink)		
825	and moisture advection (orange) at the SCS are also marked.		
826	FIG. 21. Schematics for synoptic conditions favorable for the formation of lee vortices to the		
827	west of Sumatra that may subsequently develop into TCs in the IO during the post-		
828	monsoon period (Oct-Dec), obtained in this study. These factors include vorticity and		
829	moisture advection from the SCS (linked to TC remnant or BV), prevailing northeasterly		
830	(southeasterly) winds in NH (SH), and the deflection of low-level northeasterly wind by		
831	the northern part (westerly wind by the southern part) of Sumatra for the northern		
832	(southern) vortex.		

TABLE 1. The CReSS model domain configuration (top), initial and boundary conditions (IC/BCs, middle), and physical schemes (bottom) used in this study.

834

Cases	Nisha (2008)	Ward and Cleo (2009)	
Projection	Mercater, center at 100°E		
Grid spacing (km)	4.0 × 4.0 × 0.1-0.727 (0.5)*		
Grid dimension (x, y, z) and domain size (km)	$1400 \times 1116 \times 40 \ (5600 \times 4464 \times 20)$		
IC/BCs (including SST)	ECMWF-YOTC analyses (0.25°, 20 levels, every 6 h)		
Topography	Digital elevation model at (1/120)°		
Initial time	1200 UTC 14 Nov 2008	0000 UTC 29 Nov 2009	
Integration length	15 days	16 days	
Output frequency	1 h		
Cloud microphysics	Bulk cold-rain (Lin et al. 1983; Cotton et al. 1986; Murakami 1990; Ikawa and Saito 1991; Murakami et al. 1994)		
PBL/turbulence	1.5-order closure with prediction of turbulent kinetic energy (Deardorff 1980; Tsuboki and Sakakibara 2007)		
Surface processes	Energy/momentum fluxes, shortwave and longwave radiation (Kondo 1976; Louis et al. 1982; Segami et al. 1989)		
Substrate model	43 levels, every 5 cm to 2.1 m		

^{*} The vertical grid spacing (Δz) of CReSS is stretched (smallest at the bottom), and the
averaged spacing is given in the parentheses.

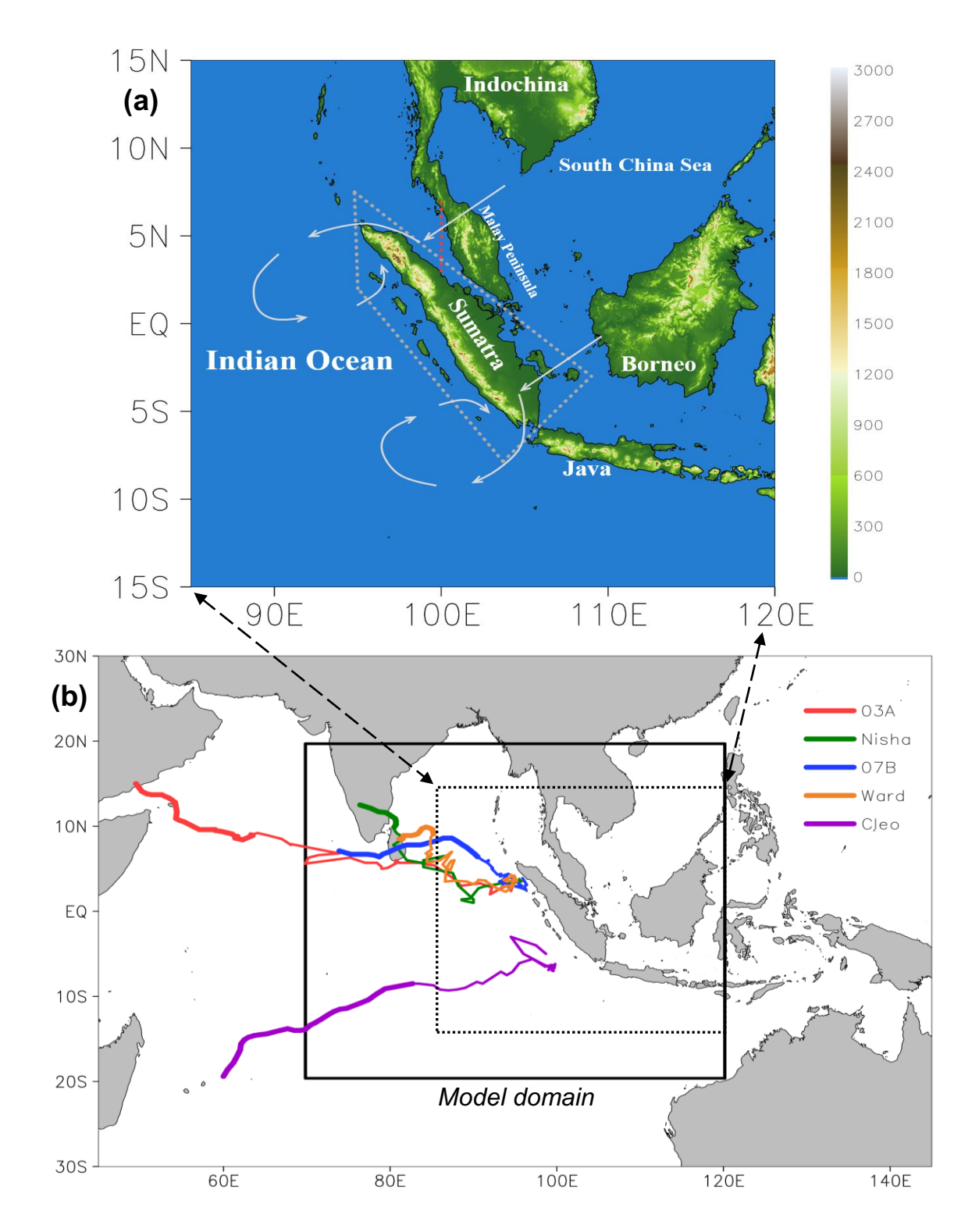


FIG. 1. (a) The topography of Sumatra and surrounding region (m, color), and a schematic of lee vortices based on Kuettner (1967). The gray-dotted polygon shows the area to remove terrain in sensitivity tests, and the red-dotted line shows the segment used to compute Fr. (b) Tracks of the five selected cases (thickened for lifespan reaching TS intensity) and the model simulation domain (thick solid box).

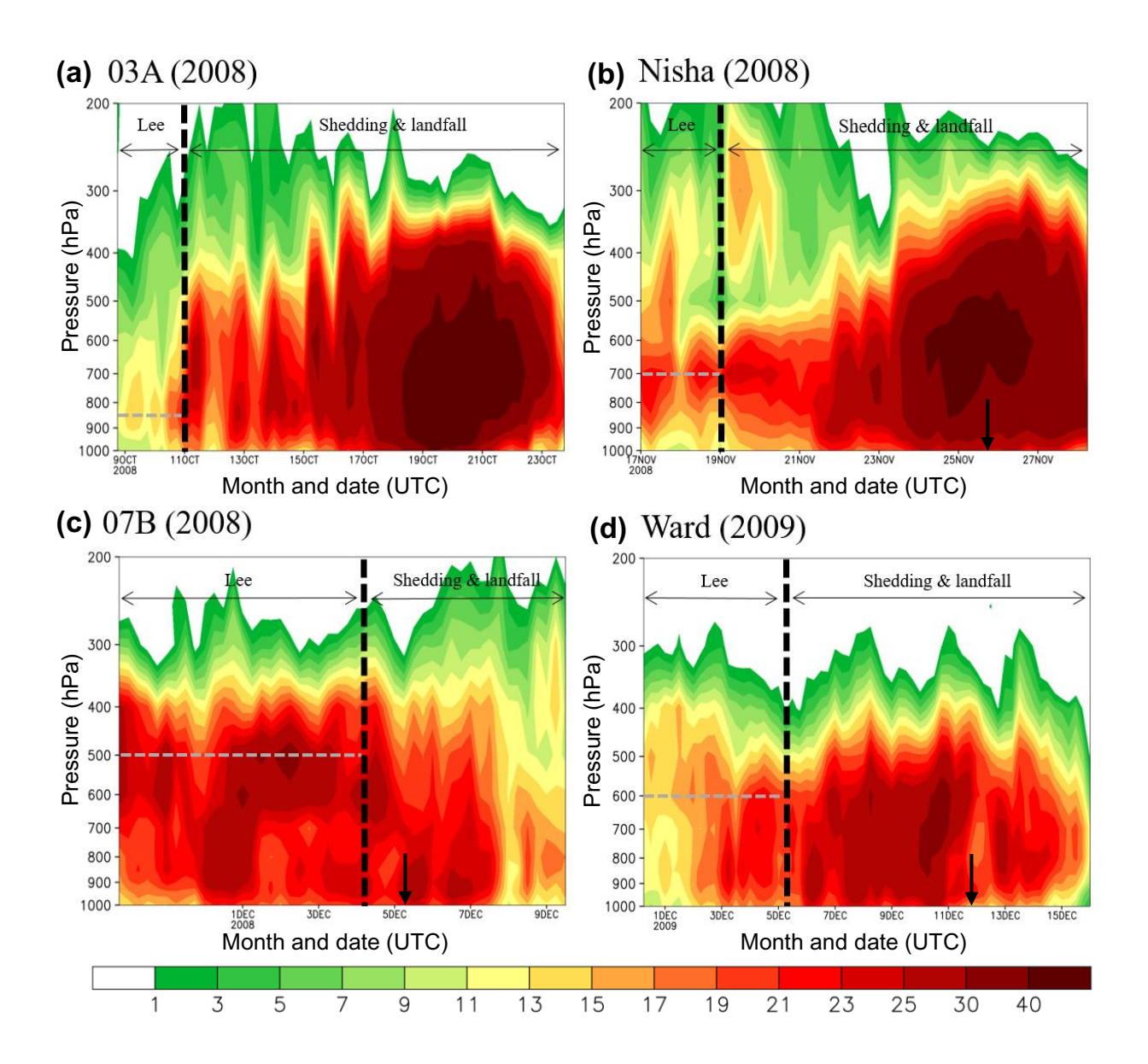


FIG. 2. Time-height section of mean relative vorticity (ζ , 10^{-6} s⁻¹), computed from ECMWF-YOTC data and averaged inside 550 km from the vortex center, for the four cases in NIO: (a) 03A, (b) Nisha, (c) 07B, and (d) Ward. Each panel starts at the time of lee vortex formation. The thick dashed vertical lines mark the time when the vortex started to move downstream and the arrows denote when the TS intensity is reached in JTWC best-track data (not applicable for 03A). The gray dashed horizontal lines depict the level of maximum vorticity.

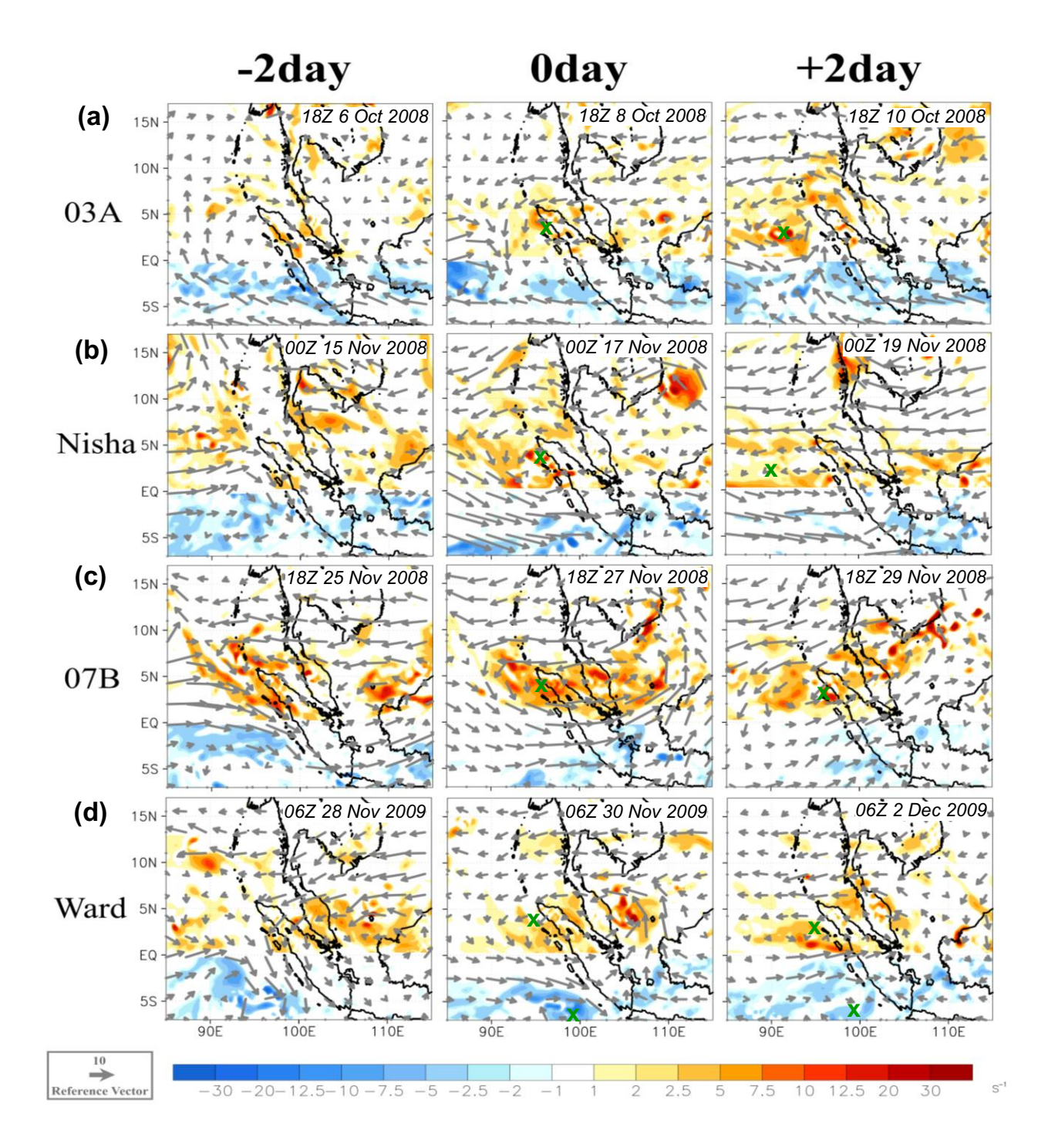


FIG. 3. Distributions of horizontal wind (gray vectors, m s⁻¹) and relative vorticity (10⁻⁵ s⁻¹, color, cyclonic only) in ECMWF-YOTC data two days before (left), at the time (middle) of, and two days after (right) the formation of the lee vortex for (a) 03A at 850 hPa, (b) Nisha at 700 hPa, (c) 07B at 500 hPa, and (d) Ward at 600 hPa. Both the reference vector and color scales are plotted at the bottom. The vortex centers at 850 hPa are marked by a green "x" [not necessarily the same as the center at the level shown in (b)-(d)].

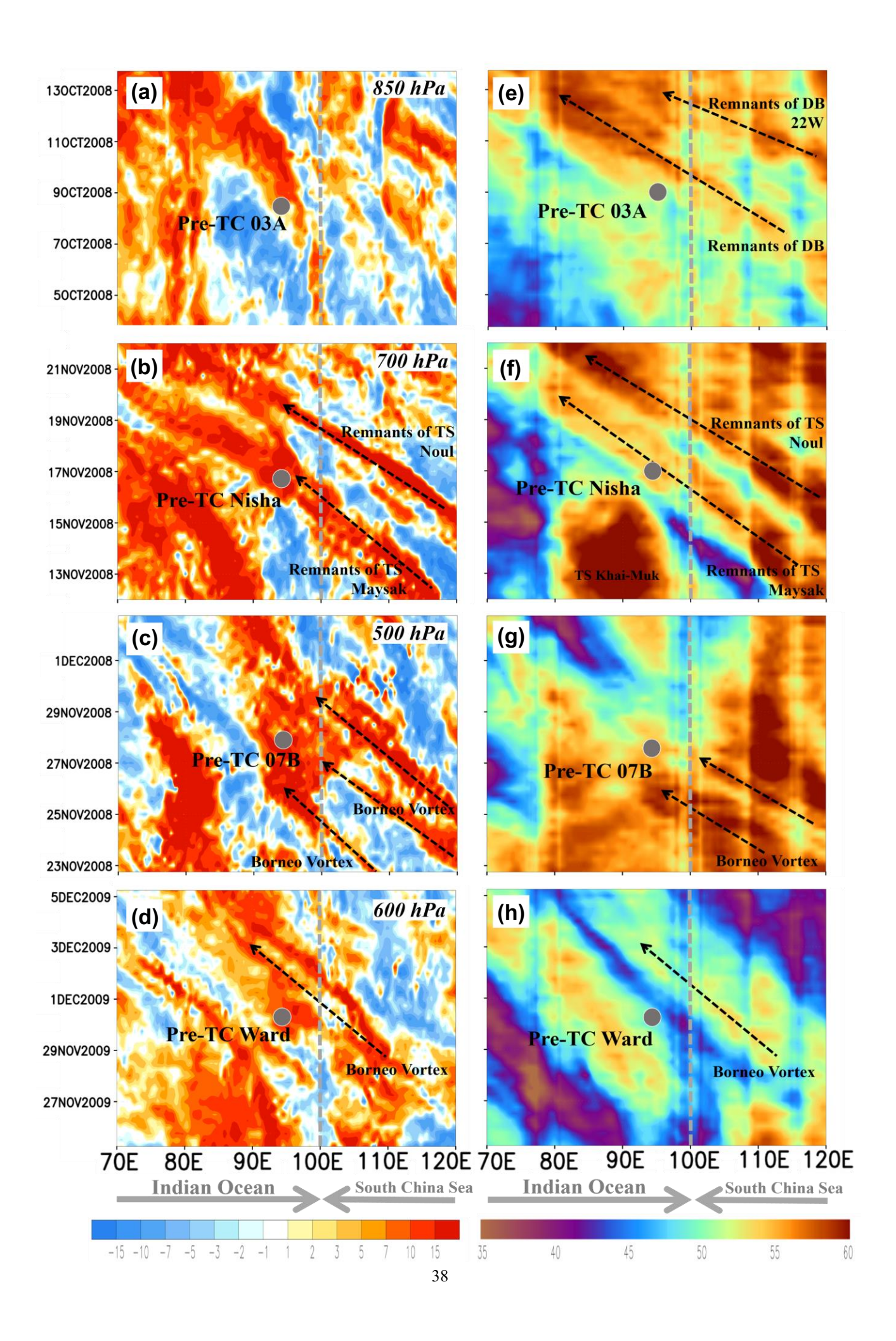


FIG. 4. Longitude-time (Hovmoller) diagrams of mean (a)-(d) relative vorticity (10⁻⁵ s⁻¹) at the pressure level as labeled (same as in Fig. 3) and (e)-(h) total column-integrated precipitable water (mm) in ECMWF-YOTC data during the case period of 03A, Nisha, 07B, and Ward, respectively (from top to bottom). The latitudinal range of averaging is 0°-15°N. The circles depict the time of lee vortex formation, a disturbance is depicted as "DB", and the vertical dashed lines near 100°E mark the boundary between the IO and the SCS.

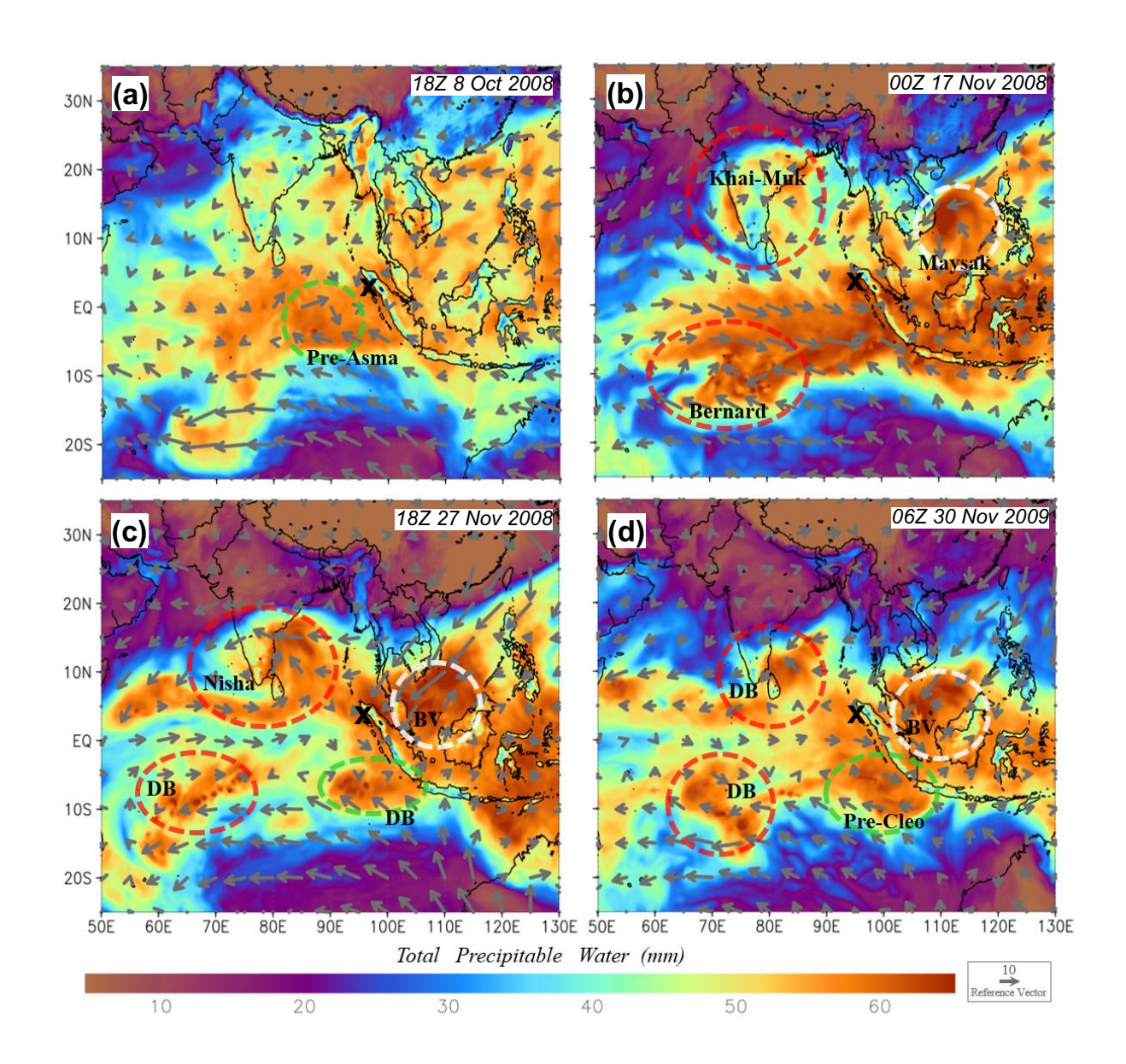


FIG. 5. Distribution of total column-integrated precipitable water (mm, color) and horizontal wind at 925 hPa (m s⁻¹, gray vectors) at the time of lee vortex formation for (a) 03A, (b) Nisha, (c) 07B, and (d) Ward, respectively. The vortex centers (at 850 hPa) are marked by an "x". The red dashed circles depict TC or disturbance (DB) in the IO, green dashed circles depict TD or pre-TC in SIO, and white dashed circles depict BV or TC remnant in the SCS. Both the reference vector and color scales are plotted at the bottom.

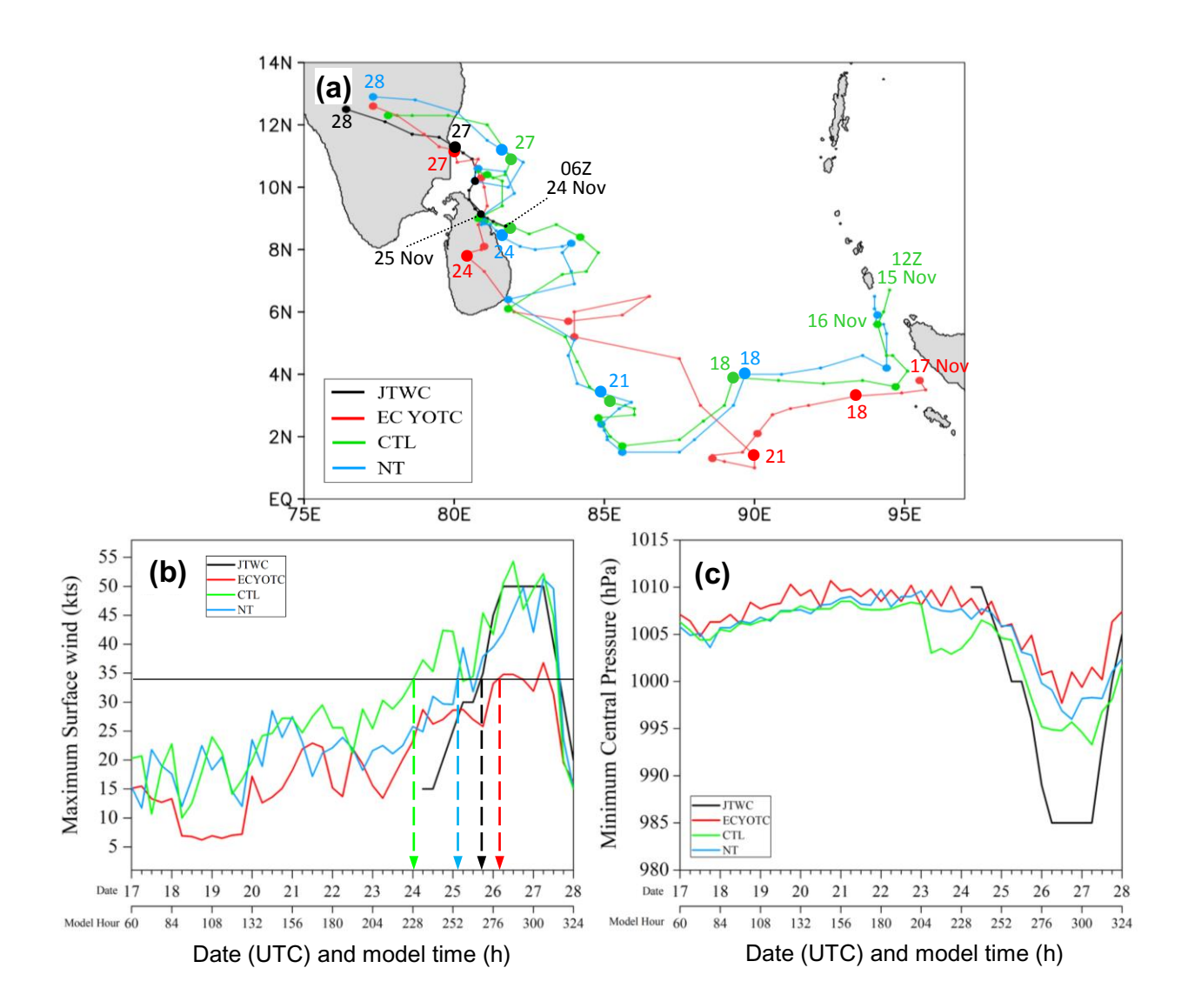


FIG. 6. Comparison of (a) track, (b) maximum surface wind speed (kts, at 10 m above the surface), and (c) central mean sea-level pressure (hPa) among JTWC best track, ECMWF-YOTC, and CTL and NT experiments for the case of Nisha (16 to 28 Nov 2008). The vortex center positions (at or near 850 hPa) are given by small dots every 6 h, median dots at 0000 UTC, and large dots every three days with dates labeled (unless not necessary) in (a). Track endpoints are also labeled (with time if not at 0000 UTC). In (b), TS intensity (34 kts) and the time to reach it in the four data sources are marked.

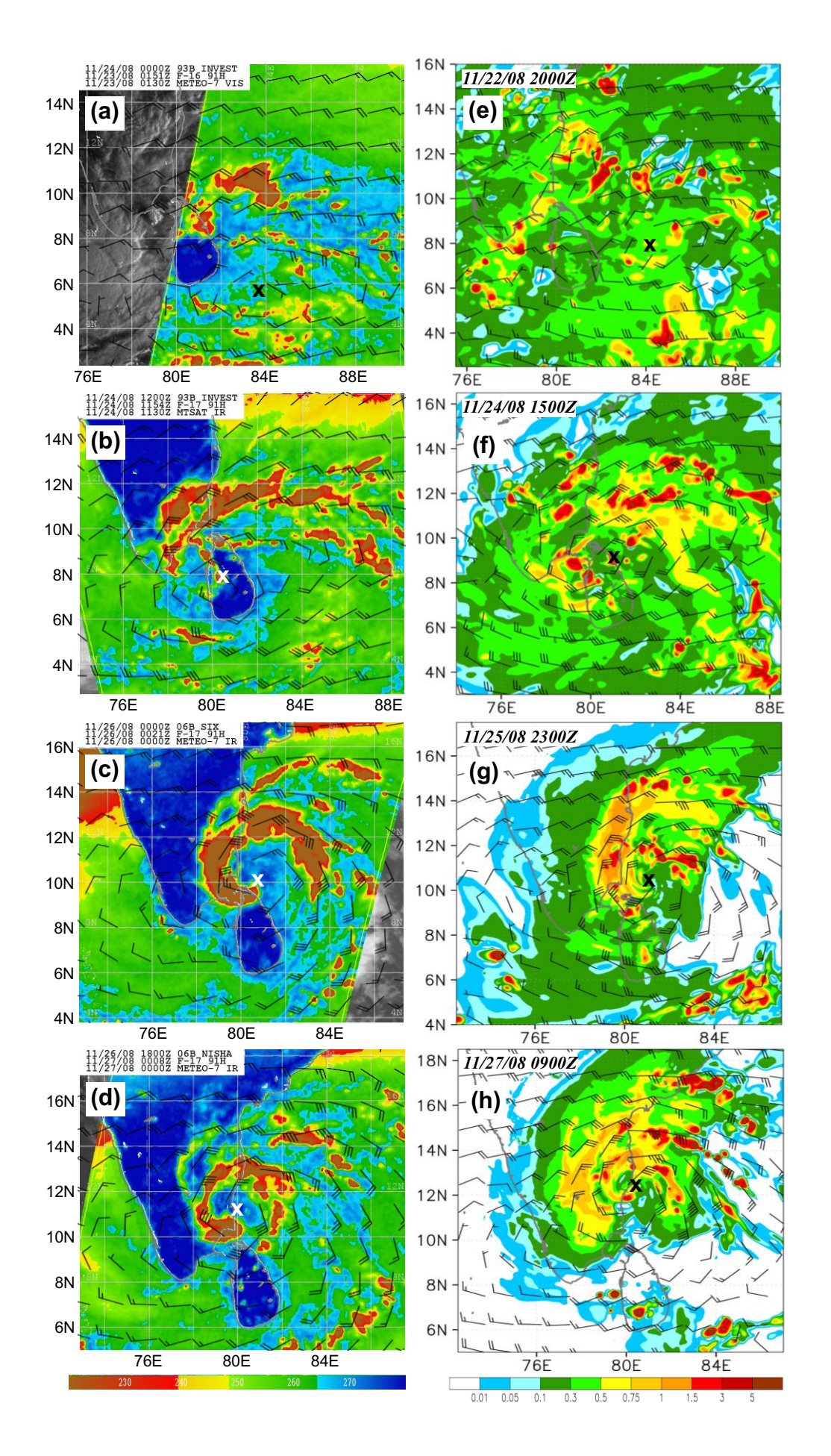


FIG. 7. (a)-(d) SSMI 91-GHz imagery of brightness temperature (*T_B*, K, color) of Nisha at (a) 0151 UTC 23, (b) 1154 UTC 24, (c) 0021 UTC 26, and (d) 0008 UTC 27 Nov 2008 (source: NRL), overlaid with ECMWF-YOTC wind fields (kts, 1 full barb = 10 kts) at 850 hPa at the closest time with data (every 6 h). (e)-(h) Column maximum mixing ratio of precipition (g kg⁻¹, rain + snow + graupel) and horizontal wind at 1547 m (kts) in CTL at (e) 2000 UTC 22, (f) 1500 UTC 24, (g) 2300 UTC 25, and (h) 0900 UTC 27 Nov, respectively. The color scales are plotted at the bottom, and the storm center is marked by an "x".

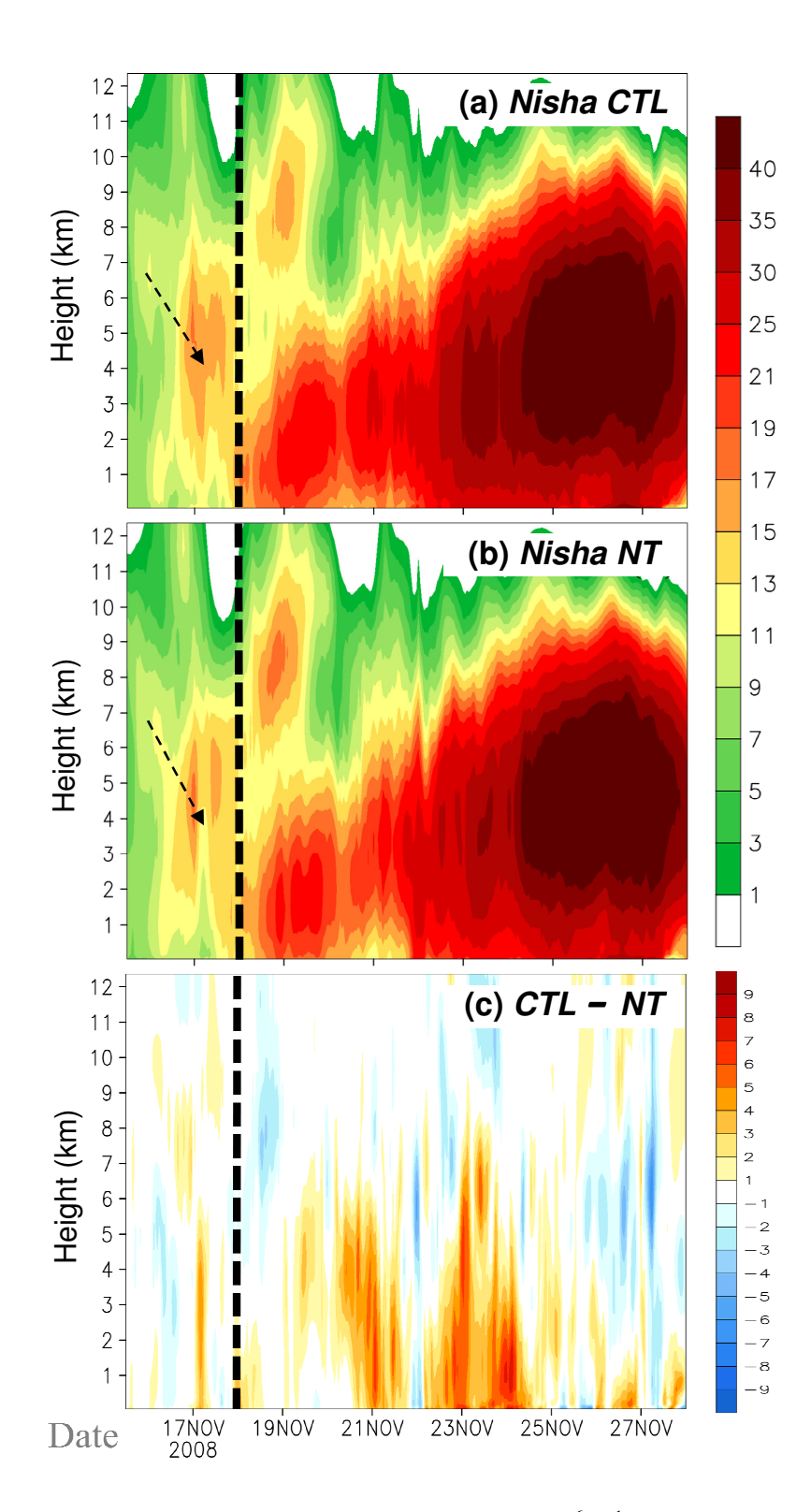


FIG. 8. Time-height section of mean relative vorticity (ζ , 10^{-6} s⁻¹) for Nisha similar to Fig. 2b, except from (a) CTL and (b) NT experiment, and (c) their difference (CTL – NT). Downward developments during the lee stage are marked.

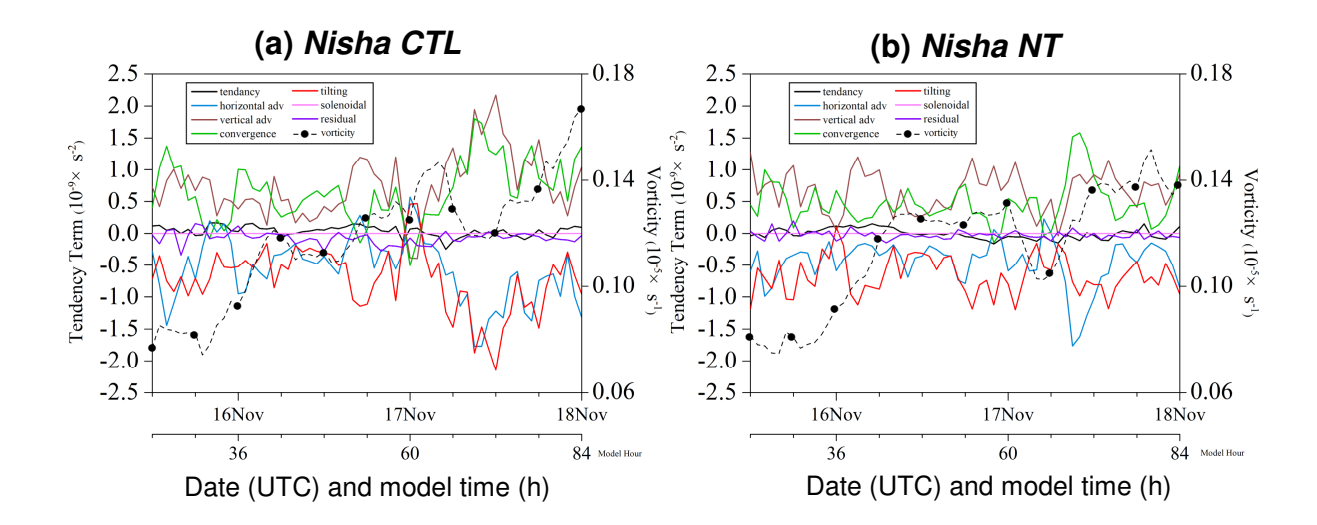


FIG. 9. The vorticity-tendency budget terms (10⁻⁹ s⁻², left axis), including local tendency, horizontal advection, vertical advection, convergence, tilting, solenoidal, and residual terms (see legend), and the mean vorticity (10⁻⁵ s⁻¹, dashed with dots, right axis) at the height of 1547 m, averaged inside 550 km, for Nisha from 1200 UTC 15 Nov to 0000 UTC 18 Nov 2008 in (a) CTL and (b) NT experiment.

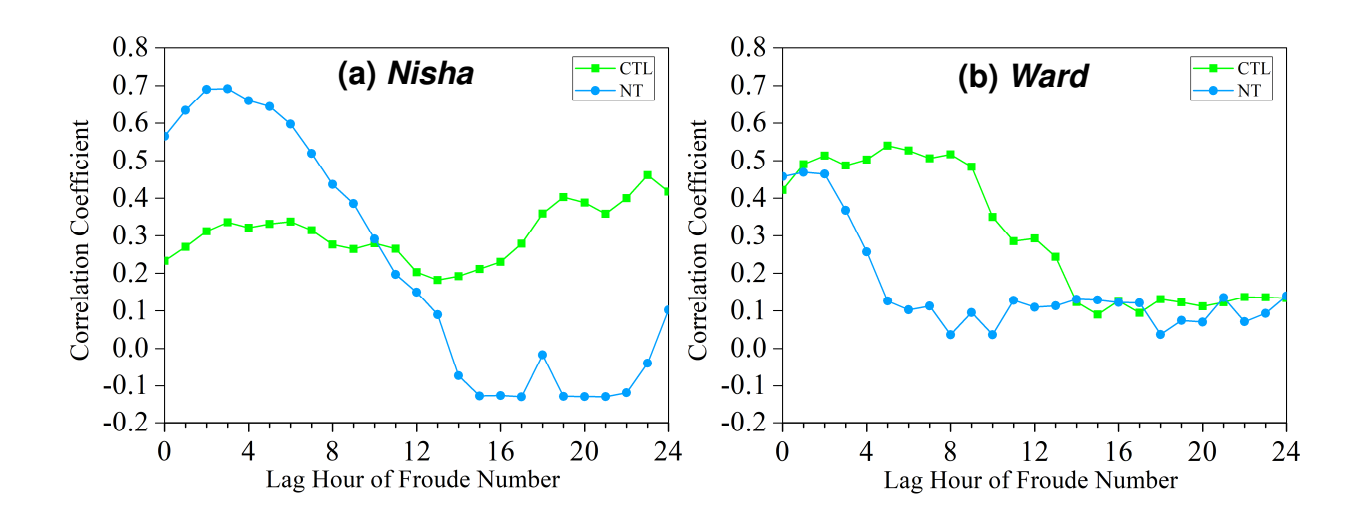


FIG. 10. The correlation coefficients between Fr and lagged mean vorticity tendency (as in Figs. 9 and 14), as a function of lagged time (h) in CTL and NT experiments for the case of (a) Nisha and (b) Ward, respectively.

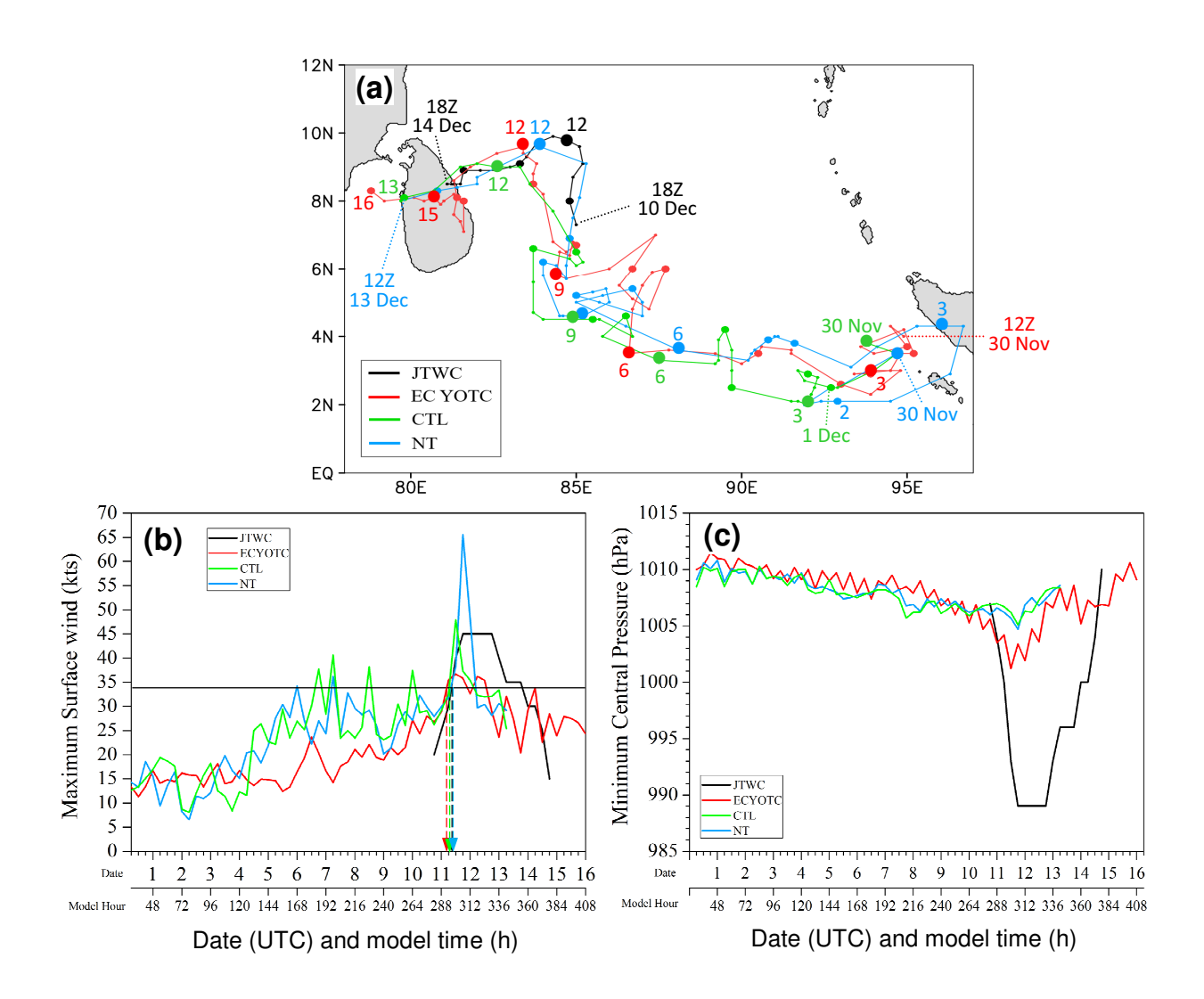


FIG. 11. As in Fig. 6, except for the case of TC Ward (30 Nov to 16 Dec 2009).

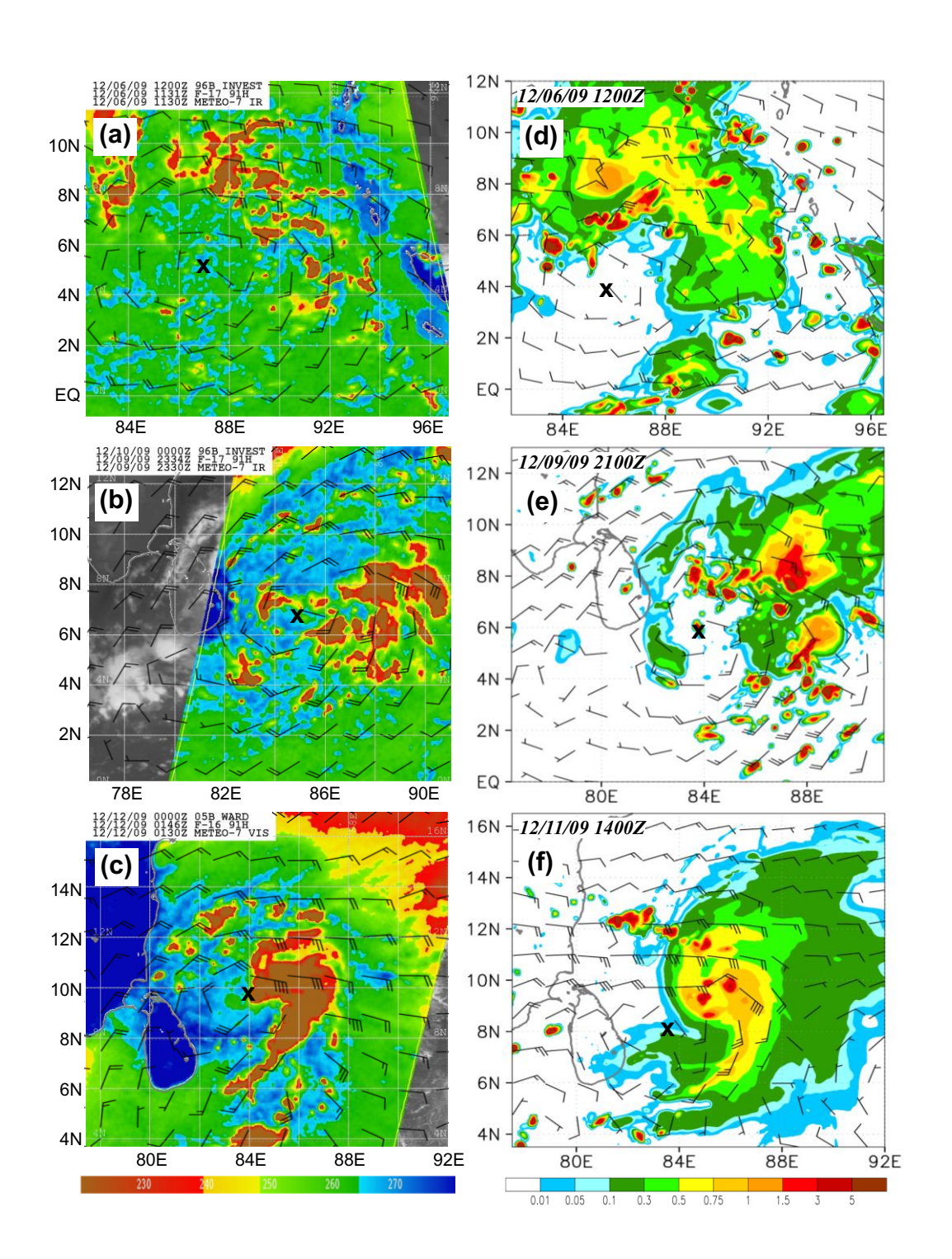


FIG. 12. As in Fig. 7, except for Ward at (a) 1130 UTC 6, (b) 2334 UTC 9, and 0146 UTC 12 Dec 2009 (source of satellite imagery: NRL), and (d) 1200 UTC 6, (e) 2100 UTC 9, and (f) 1400 UTC 12 Dec from CTL at a similar stage as in (a)-(c), respectively.

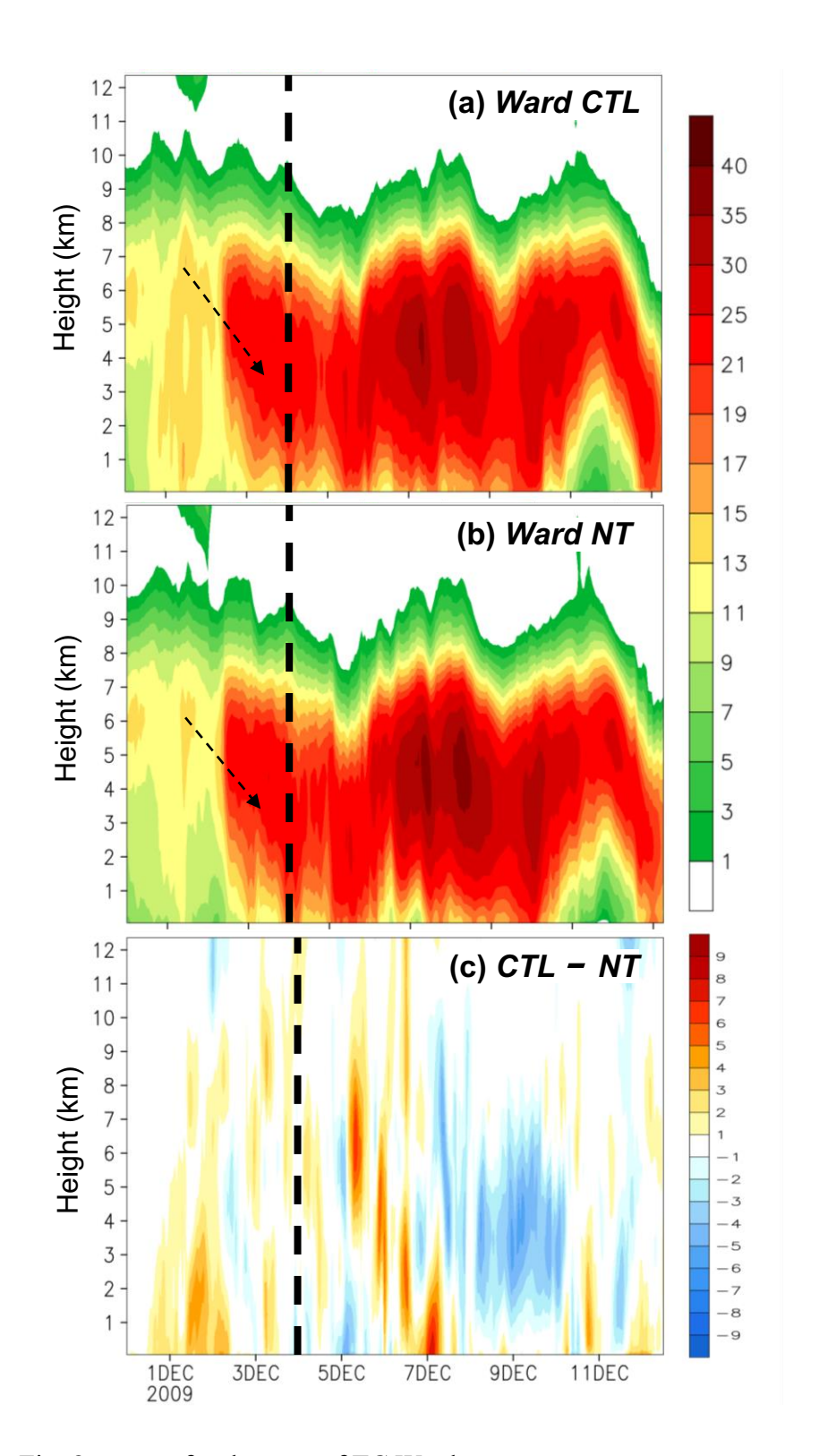


Fig. 13. As in Fig. 8, except for the case of TC Ward.

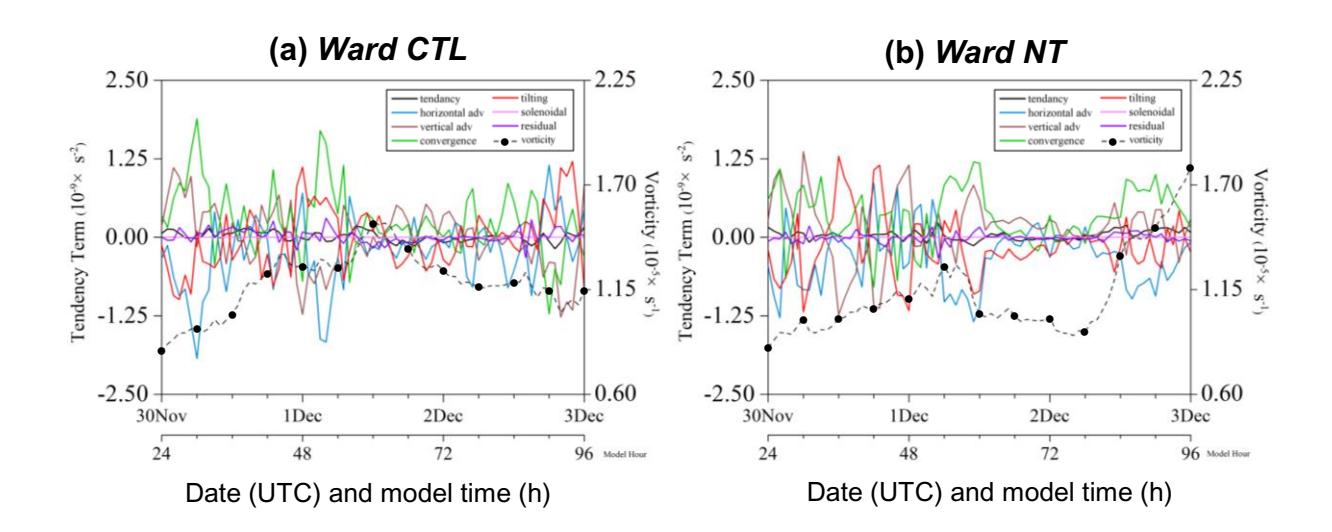


FIG. 14. As in Fig. 9, except for Ward from 0000 UTC 30 Nov to 0000 UTC 3 Dec 2009.

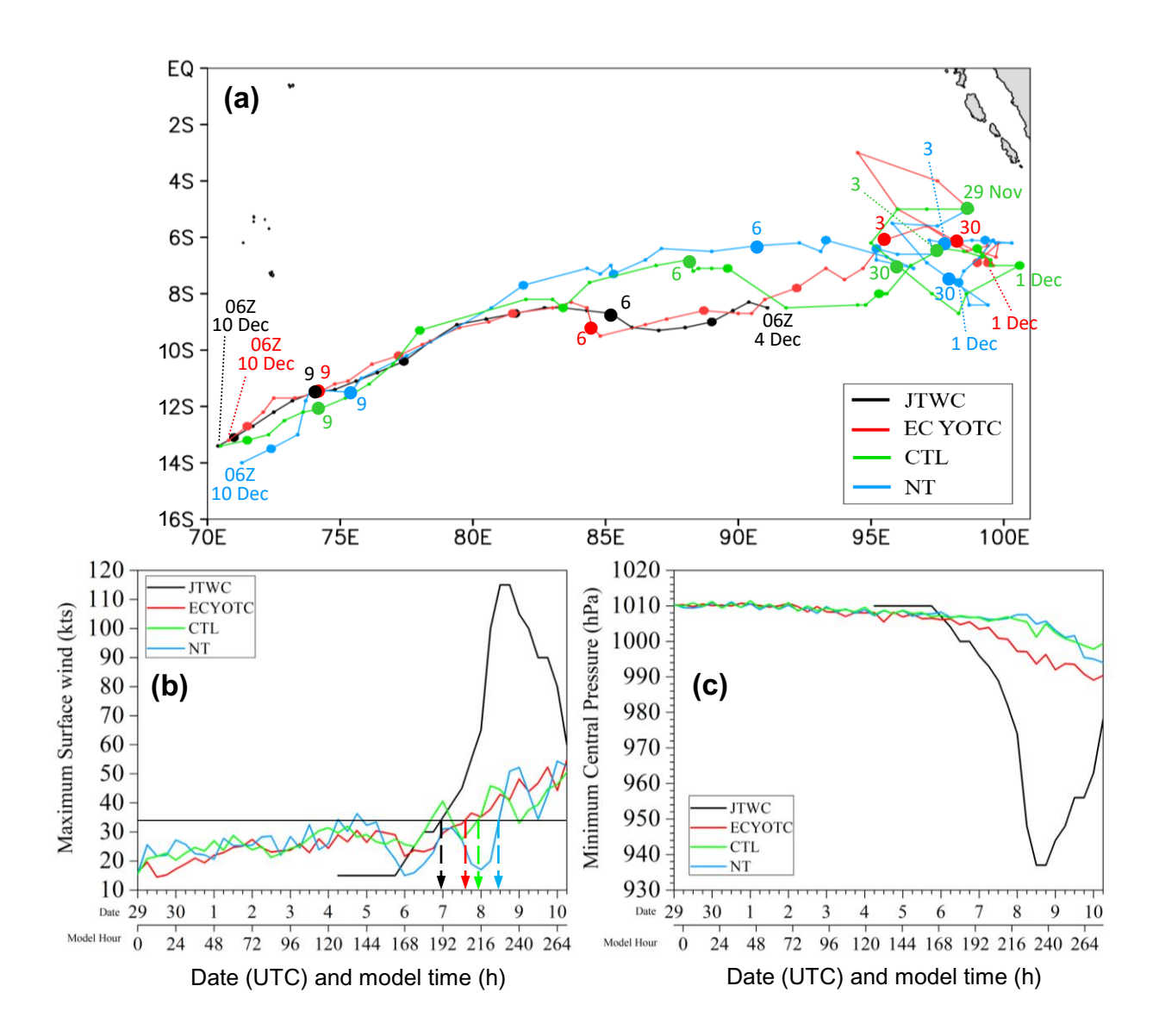


FIG. 15. As in Fig. 6, except for the case of TC Cleo (29 Nov to 10 Dec 2009).

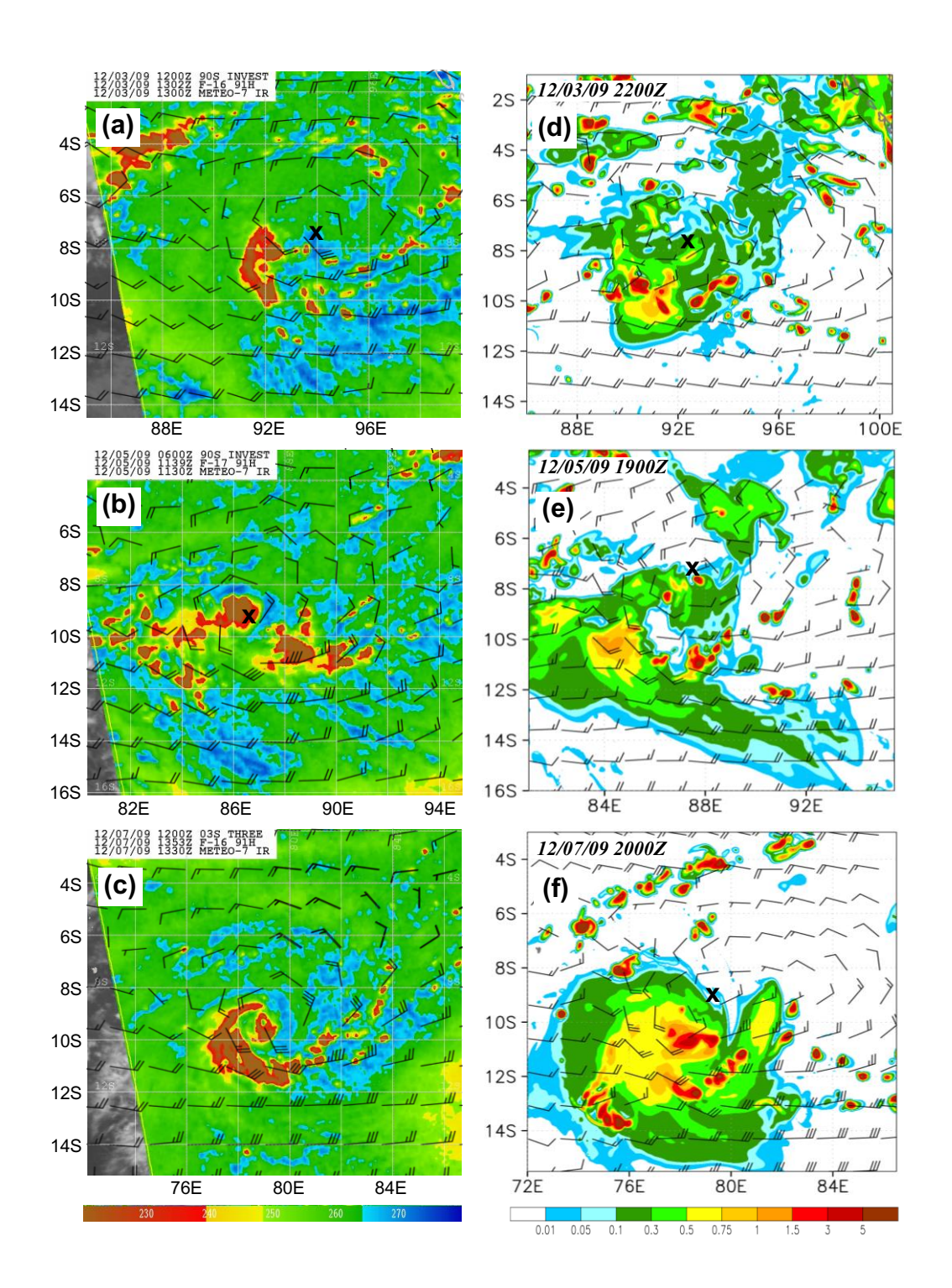


FIG. 16. As in Fig. 7, except for Cleo at (a) 1302 UTC 3, (b) 1139 UTC 5, and (c) 1353 UTC 7 Dec 2009 (source of satellite imagery: NRL), and (d) 2200 UTC 3, (e) 1900 UTC 5, and (f) 2000 UTC 7 Dec from CTL at a similar stage as in (a)-(c), respectively. The storm center in (c) is not marked for clarity.

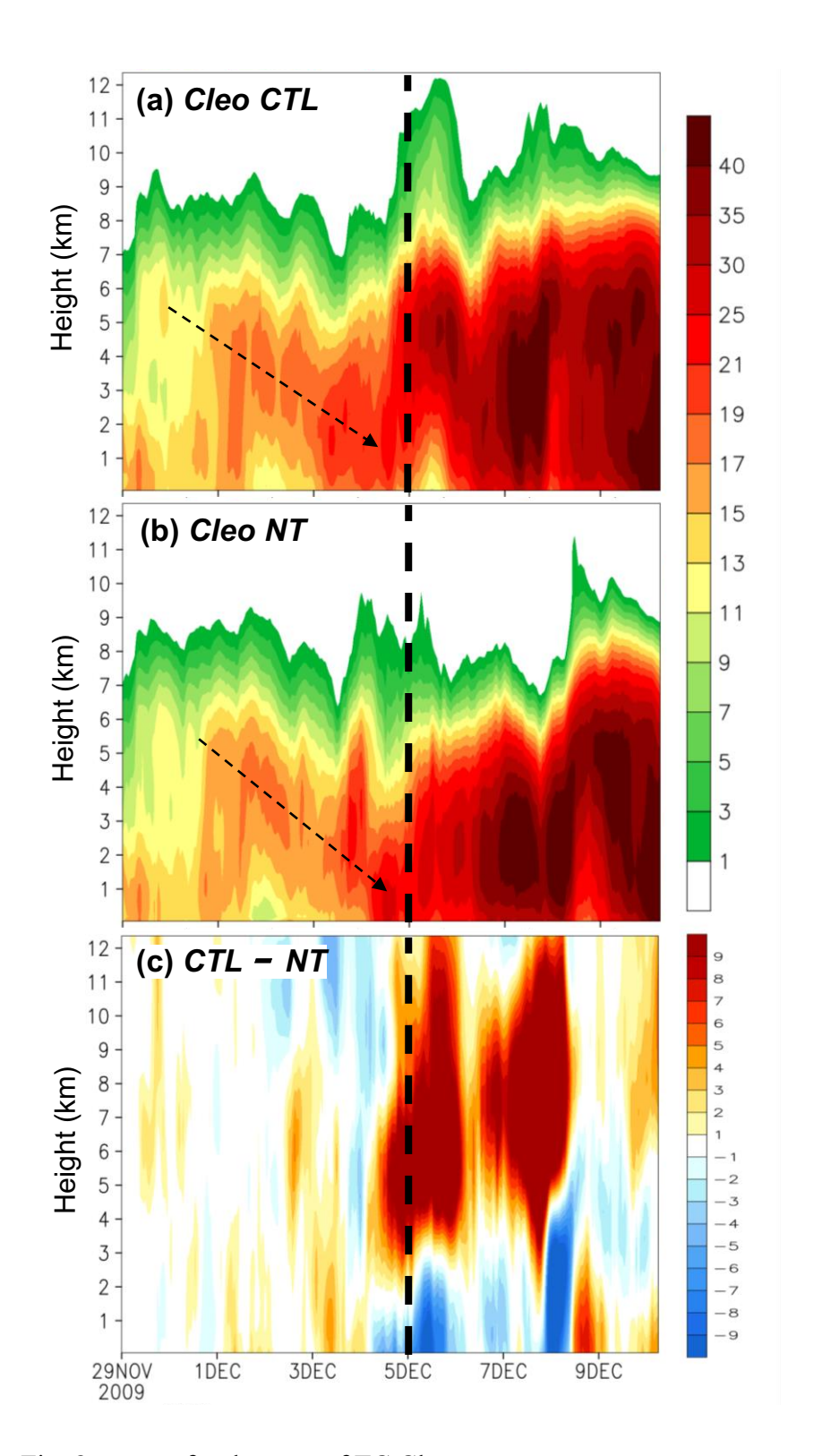


FIG. 17. As in Fig. 8, except for the case of TC Cleo.

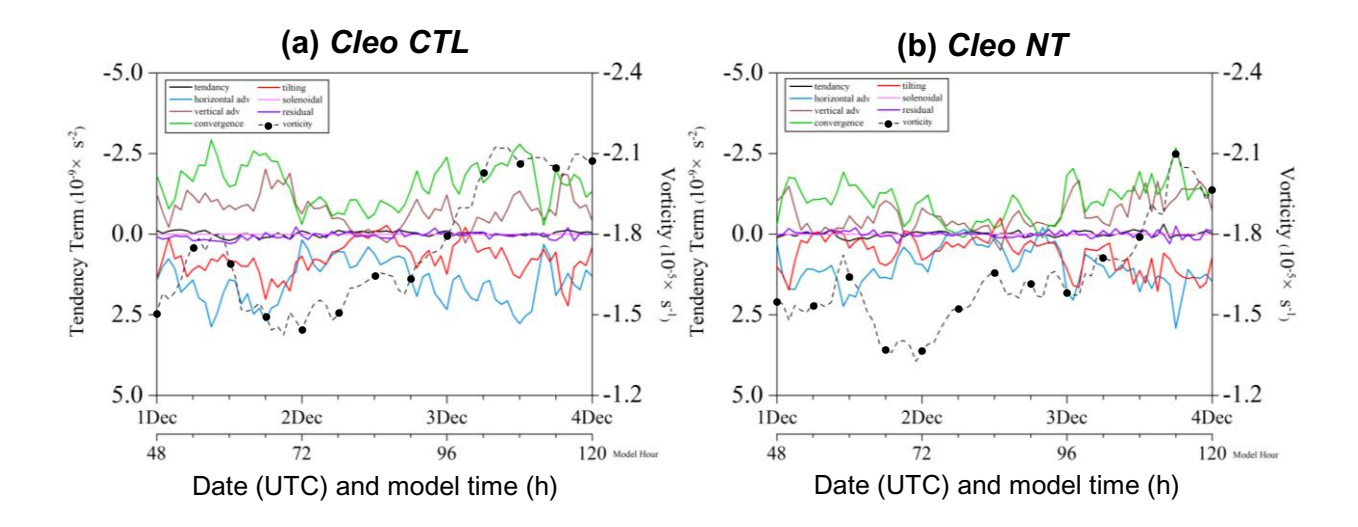


FIG. 18. As in Fig. 9, except for Cleo from 0000 UTC 1 Dec to 0000 UTC 4 Dec 2009. Note that the vertical scale is reversed for this case in the Southern Hemisphere.

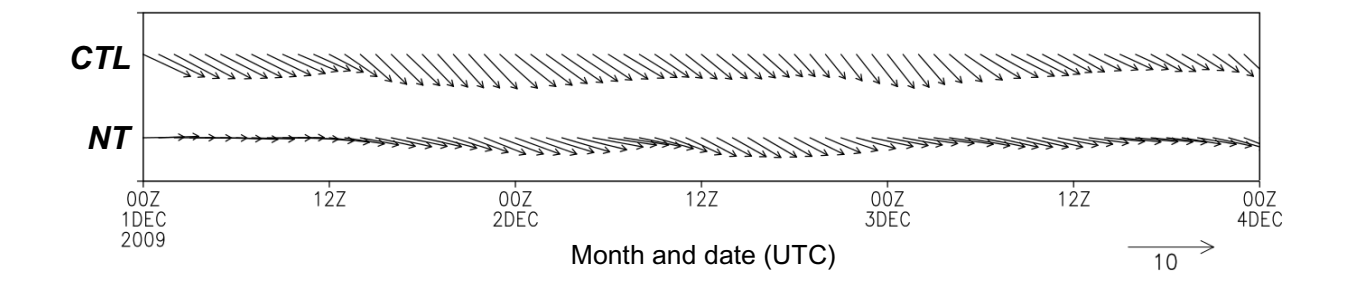


FIG. 19. Averaged low-level horizontal wind (m s $^{-1}$, over 50-1913 m) in the northeastern quadrant of Cleo at 1-h intervals from 0000 UTC 1 Dec to 0000 UTC 4 Dec 2009 in CTL and NT experiments.

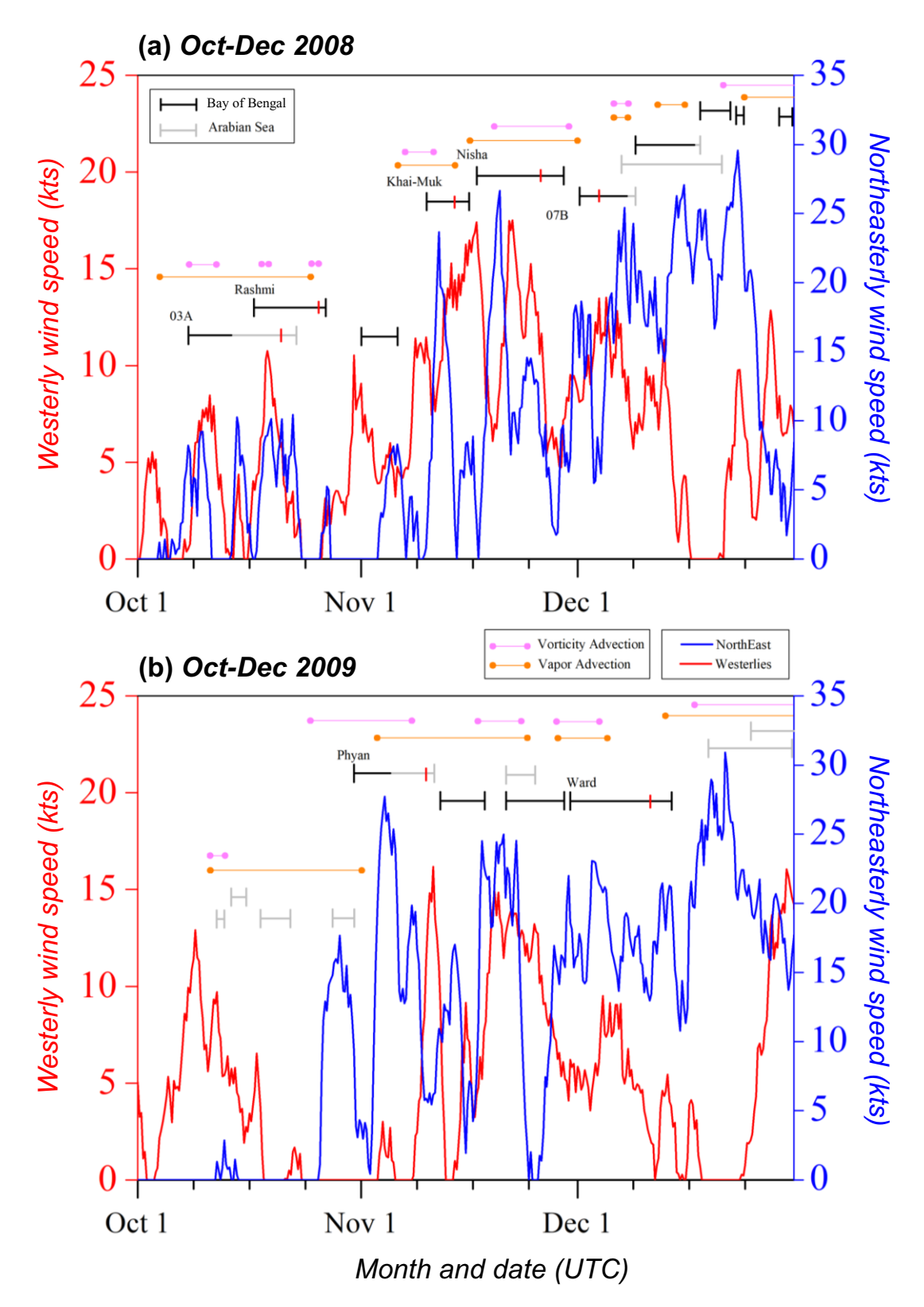


FIG. 20. Time-series of westerly wind speed in equatorial IO (kts, red, averaged over 5°S-5°N, 80°-90°E) and northeasterly wind speed east of northern Sumatra (kts, blue, averaged over 5°-10°N, 107°-115°E) at 925 hPa in the ECMWF-YOTC data during Oct-Dec of (a) 2008 and (b) 2009. Black/gray segments indicate periods with a closed vortex in

BOB/Arabian Sea (divided at 80°E) with named storms labeled (the naming times shown by short red ticks). The periods with 700-hPa positive vorticity advection (pink) and moisture advection (orange) at the SCS are also marked.

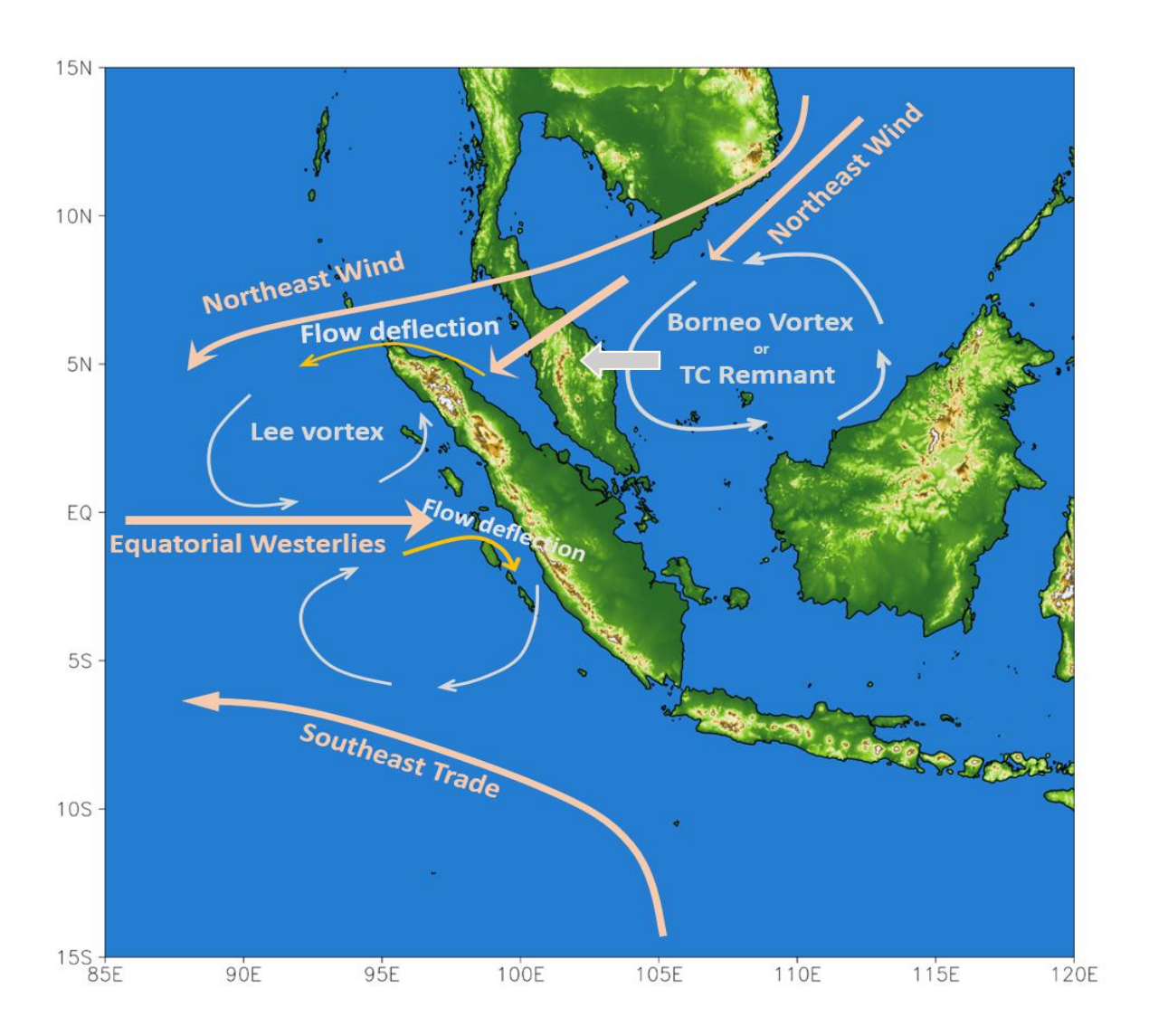


FIG. 21. Schematics for synoptic conditions favorable for the formation of lee vortices to the west of Sumatra that may subsequently develop into TCs in the IO during the post-monsoon period (Oct-Dec), obtained in this study. These factors include vorticity and moisture advection from the SCS (linked to TC remnant or BV), prevailing northeasterly (southeasterly) winds in NH (SH), and the deflection of low-level northeasterly wind by the northern part (westerly wind by the southern part) of Sumatra for the northern (southern) vortex.